

AERONAUTICS INSTITUTE OF TECHNOLOGY



Felipe Mello dos Reis

**DEVELOPMENT OF ONE-PART ALKALI-ACTIVATED
CEMENT WITH LOW-CALCIUM SOLID PRECURSORS
AND ALTERNATIVE ALKALINE SOURCES.**

Final Paper
2025

Course of Civil-Aeronautics Engineering

CDU ????

Felipe Mello dos Reis

**DEVELOPMENT OF ONE-PART ALKALI-ACTIVATED
CEMENT WITH LOW-CALCIUM SOLID PRECURSORS
AND ALTERNATIVE ALKALINE SOURCES.**

Advisor

Prof. Dr. João Cláudio Bassan de Moraes (ITA)

Co-advisor

Pamela Rodrigues Passos Severino (ITA)

CIVIL-AERONAUTICS ENGINEERING

SÃO JOSÉ DOS CAMPOS
INSTITUTO TECNOLÓGICO DE AERONÁUTICA

2025

Cataloging-in Publication Data
Documentation and Information Division

dos Reis, Felipe Mello

Development of one-part alkali-activated cement with low-calcium solid precursors and alternative alkaline sources. / Felipe Mello dos Reis.

São José dos Campos, 2025.

64f.

Final paper (Undergraduation study) – Course of Civil-Aeronautics Engineering– Instituto Tecnológico de Aeronáutica, 2025. Advisor: Prof. Dr. João Cláudio Bassan de Moraes. Co-advisor: Pamela Rodrigues Passos Severino.

1. Alkali activated material. 2. Geopolymer. 3. One-part. I. Instituto Tecnológico de Aeronáutica. II. Title.

BIBLIOGRAPHIC REFERENCE

DOS REIS, Felipe Mello. **Development of one-part alkali-activated cement with low-calcium solid precursors and alternative alkaline sources.**. 2025. 64f. Final paper (Undergraduation study) – Instituto Tecnológico de Aeronáutica, São José dos Campos.

CESSION OF RIGHTS

AUTHOR'S NAME: Felipe Mello dos Reis

PUBLICATION TITLE: Development of one-part alkali-activated cement with low-calcium solid precursors and alternative alkaline sources..

PUBLICATION KIND/YEAR: Final paper (Undergraduation study) / 2025

It is granted to Instituto Tecnológico de Aeronáutica permission to reproduce copies of this final paper and to only loan or to sell copies for academic and scientific purposes. The author reserves other publication rights and no part of this final paper can be reproduced without the authorization of the author.

Felipe Mello dos Reis
Rua H8A, Ap. 113
12.228-460 – São José dos Campos–SP

DEVELOPMENT OF ONE-PART ALKALI-ACTIVATED CEMENT WITH LOW-CALCIUM SOLID PRECURSORS AND ALTERNATIVE ALKALINE SOURCES.

This publication was accepted like Final Work of Undergraduation Study

Felipe Mello dos Reis
Author

João Cláudio Bassan de Moraes (ITA)
Advisor

Pamela Rodrigues Passos Severino (ITA)
Co-advisor

Prof^a. Dr^a. Cláudia Azevedo Pereira
Course Coordinator of Civil-Aeronautics Engineering

São José dos Campos: maio 26, 2025.

Resumo

Na busca por alternativas mais sustentáveis ao cimento Portland, os cimentos ativados alcalinamente têm sido amplamente estudados. Inicialmente, a maioria dos processos de mistura ocorre em duas etapas, que sacrificam a eficiência produtiva em função das melhores propriedades mecânicas. Com o objetivo aumentar a escalabilidade do processo, o desenvolvimento de sistemas monocomponentes trouxe uma tecnologia mais acessível e prática para a indústria. Ainda assim, os estudos atuais se concentram em precursores ricos em cálcio, enquanto o uso de fontes alcalinas tradicionais apresenta desafios relacionados à segurança e ao custo. Este trabalho propõe o desenvolvimento de um cimento ativado alcalinamente monocomponente utilizando precursores sólidos de baixo teor de cálcio, como sílica ativa e metacaulim, e fontes alcalinas mais seguras e acessíveis, como carbonato de potássio e hidróxido de cálcio, garantindo resistência mecânica adequada e maior viabilidade para aplicação na construção civil.

Abstract

In the search for more sustainable alternatives to Portland cement, alkali-activated cements have been extensively studied. Initially, most mixing processes occur in two steps, which sacrifice productive efficiency in favor of improved mechanical properties. Aiming to increase process scalability, the development of one-part (just-add-water) systems has brought a more accessible and practical technology to the industry. Nonetheless, current studies mainly focus on calcium-rich precursors, while the use of conventional alkaline activators raises concerns related to safety and cost. This work proposes the development of a one-part alkali-activated cement using low-calcium solid precursors, such as silica fume and metakaolin, along with safer and more affordable alkaline sources, such as potassium carbonate and calcium hydroxide. The goal is to ensure adequate mechanical performance while enhancing the viability of these materials for application in the construction industry.

List of Figures

FIGURE 2.1 – Classification of different subsets of alkali-activated materials, with comparisons to Portland cement and calcium sulfoaluminate binder chemistry. Shading indicates approximate alkali content; darker shading corresponds to higher concentrations of Na and/or K (RAKHIMOV; RAKHIMOV, 2019a).	17
FIGURE 2.2 – Scheme of the alkaline activation process (DUXSON A. FERNÁNDEZ-JIMÉNEZ, 2006).	18
FIGURE 2.3 – Ternary diagram of the most common precursors (GIERGICZNY, 2019).	18
FIGURE 2.4 – Solubility of silica and alumina as a function of pH (MASON, 1952).	21
FIGURE 4.1 – SEM micrographs of paste with Si/Al = 0.9 after 3 days of curing (spot 5).	31
FIGURE 4.2 – SEM micrographs of paste with Si/Al = 3.0 after 3 days of curing (spot 3).	32
FIGURE 4.3 – SEM micrographs of paste with Si/Al = 5.0 after 3 days of curing (spot 1).	32
FIGURE 4.4 – EDS analysis of Spot 5, Si/Al = 0.9, cured for 3 days at 60°C at 1000× magnification.	33
FIGURE 4.5 – EDS analysis of Spot 3, Si/Al = 3.0, cured for 3 days at 60°C at 1000× magnification.	33
FIGURE 4.6 – EDS analysis of Spot 1, Si/Al = 5.0, cured for 3 days at 60°C at 1000× magnification.	34
FIGURE 4.7 – XRD patterns of pastes at different Si/Al ratios after 3 days of curing.	35
FIGURE 4.8 – FTIR spectra of pastes at different Si/Al ratios after 3 days of curing.	36
FIGURE B.1 – SEM micrographs of Spot 1, Si/Al = 0.9, cured for 3 days at 60°C.	45

List of Tables

TABLE 2.1 – Characteristics of common or innovative residual materials that can be added to concrete to produce more sustainable binders (NODEHI; TAGHVAEE, 2022)	20
TABLE 3.1 – Results of physical and chemical requirements of standardized quartz sand.	24
TABLE 3.2 – Particle size distribution of the fractions of standardized quartz sand. .	24
TABLE 4.1 – Chemical composition (wt %) of the precursors: metakaolin (MK) and active silica (SA).	29
TABLE 4.2 – Summary of XRD phase observations for precursors and alkaline sources.	30
TABLE 4.3 – EDS spectrum of pastes after 3 days of curing at 60°C.	34
TABLE 4.4 – Semi-quantitative crystalline phases at 3 days for different Si/Al ratios (XRD).	35
TABLE 4.5 – Assignment of FTIR absorption bands observed in pastes after 3 days of curing at 60°C, where T = Si or Al.	37
TABLE A.1 – Mix design formulations for paste samples with varying Si/Al ratios. .	43
TABLE A.2 – Mix design formulations for mortar samples with varying Si/Al ratios. .	43
TABLE C.1 – EDS spectrum of Si/Al = 0.9 pastes after 3 days of curing at 60°C. .	62
TABLE C.2 – EDS spectrum of Si/Al = 3.0 pastes after 3 days of curing at 60°C. .	62
TABLE C.3 – EDS spectrum of Si/Al = 5.0 pastes after 3 days of curing at 60°C. .	63

List of Abbreviations and Acronyms

CO_2	carbon dioxide
GHG	greenhouse gases
AAM	alkali-activated materials
SiO_2	silica
Al_2O_3	alumina
N-A-S-H	sodium aluminate silicate hydrate
C-A-S-H	calcium aluminate silicate hydrate
K_2CO_3	potassium carbonate
$Ca(OH)_2$	calcium hydroxide
MK	metakaolin
SF	silica fume
IPT	Institute for Technological Research
ITA	Aeronautics Institute of Technology
EDS	Energy dispersive X-ray spectroscopy
XRD	X-ray diffraction
OH^-	hydroxyl
FTIR	Fourier transform infrared spectroscopy
ABNT	Brazilian Association of Technical Standards
NBR	Brazilian Standard
ASTM	American Society for Testing and Materials
OPC	Ordinary Portland Cement
GGBFS	Ground Granulated Blast Furnace Slag
MSWIA	Municipal Solid Waste Incineration Ash
NaOH	sodium hydroxide
Na_2SiO_3	sodium silicate
KOH	potassium hydroxide
Na_2CO_3	sodium carbonate
PSD	particle size distribution
LOI	loss on ignition

MIP mercury intrusion porosimetry

List of Symbols

w/s Water/solids ratio
s/b Sand/binder ratio

Contents

1	INTRODUCTION	14
2	LITERATURE REVIEW	16
2.1	Historical Context	16
2.2	Raw Materials for AAM	17
2.2.1	Precursors	17
2.2.2	Activators	21
2.3	Environmental Impacts	22
2.4	Mechanical Properties	22
3	METHODOLOGY	23
3.1	Materials	23
3.2	Methods	24
3.2.1	Production and Characterization of Raw Materials	24
3.2.2	Production of Geopolymeric Pastes and Mortars	25
3.2.3	Microstructural studies and Mechanical tests of hardened state	27
4	RESULTS AND DISCUSSION	29
4.1	Chemical and Physical Characterization of Precursors	29
4.1.1	Chemical Composition of Precursors	29
4.1.2	X-Ray Diffraction of Precursors and Alkaline Sources	30
4.2	Microstructural Characterization of Pastes	31
4.2.1	Scanning Electron Microscopy and Energy Dispersive Spectroscopy .	31
4.2.2	X-Ray Diffraction	34

4.2.3 Fourier Transform Infrared Spectroscopy	36
5 CONCLUSION	38
BIBLIOGRAPHY	39
APPENDIX A – MIX DESIGN FORMULATIONS	43
APPENDIX B – SEM IMAGES	44
B.1 Si/Al = 0.9	45
B.2 Si/Al = 3.0	50
B.3 Si/Al = 5.0	56
APPENDIX C – EDS SPECTRA	62
C.1 Si/Al = 0.9	62
C.2 Si/Al = 3.0	62
C.3 Si/Al = 5.0	63
APPENDIX D – FTIR SPECTRA	64

1 Introduction

Cement is one of the main materials in civil construction, being used from the construction of houses and buildings to bridges and highways. In developing countries such as Brazil, cement is widely used due to its low complexity and cost, which allows its use on a large scale in any location. The exponential increase in cement production, 10 times greater than the world population growth (United Nations, 1995), has been accompanied by a significant share of greenhouse gas (GHG) emissions, due to the calcination process of limestone that transforms calcium carbonate into calcium oxide and carbon dioxide in high-temperature furnaces. The production of Portland cement generates on average 842 kg of CO_2/t of clinker produced (ANDREW, 2018), representing 5% of anthropogenic GHG emissions (IEA; WBCSD, 2009).

In this context, there is a need to develop new cementitious materials that present three main properties: low GHG emissions, low cost, and high strength/durability (SCRIVENER *et al.*, 2018).

Alkaline-activated materials (AAM) - solid precursors rich in silica (SiO_2) and alumina (Al_2O_3), capable of forming binding gels composed of sodium-alumino-silicate hydrate (N-A-S-H) and calcium-alumino-silicate hydrate (C-A-S-H) - have gained prominence due to their potential to partially or totally replace Portland cement, significantly reducing the GHG emissions associated with conventional cement production.

There are two ways in which AAM can be produced: by mixing the solid precursor with a liquid alkaline activator or with a solid alkaline source and water. Two-part systems have been widely employed in the initial development of this market due to their high mechanical performance, durability, and chemical resistance. However, one-part systems are a more scalable technology due to the lower risk of handling and storing of solid activators (PROVIS, 2018).

Calcium-rich solid precursors are widely used due to several advantages, such as rapid strength development (PROVIS; BERNAL, 2014), reduced reliance on thermal curing (KE *et al.*, 2021), and the formation of denser and less porous matrices by C-A-S-H reaction products compared to N-A-S-H gels (BERNAL *et al.*, 2014). In this context, there remains a technical and scientific gap in the formulation and characterization of low-calcium AAMs

using alternative alkaline sources, as most studies focus on blast furnace slag as a precursor and rely on hydroxides and silicates as activators (ZAREECHIAN *et al.*, 2023).

This work proposes the development of a one-part alkaline-activated cement focusing on low-calcium solid precursors, specifically metakaolin and silica fume, combined with safer and more accessible alternative alkaline sources, such as potassium carbonate (K_2CO_3) and calcium hydroxide ($Ca(OH)_2$). This approach aims to contribute to the formulation of more sustainable, safe, and adequately performing binders for applications in civil construction, aligning with contemporary guidelines for low environmental impact (BRASIL, 2016).

2 Literature Review

2.1 Historical Context

The synthesis of materials by alkali activation began in the 1930s and 1940s, when a substitute for traditional Portland cement was developed from blast furnace slag and other aluminosilicates (PACHECO-TORGAL *et al.*, 2014). From the 1970s onwards, interest in this area increased, when the French scientist Joseph Davidovits coined the term "geopolymer" and patented several formulations. His initial studies focused on the development of inorganic, non-flammable, and fire-resistant materials (PROVIS; DEVENTER, 2009).

Since then, alkali-activated materials (AAM) have attracted the attention of researchers and industry due to their low energy consumption and sustainable nature (QIN *et al.*, 2022). Furthermore, as studies have advanced, AAMs have gained recognition for their mechanical properties and durability, as the polymerization reactions that occur during curing provide high compressive strength and resistance to chemical attack.

While the term alkali-activated materials (AAMs) broadly refers to binders produced through the reaction of aluminosilicate sources with alkaline activators, the term geopolymer defines a narrower class within this family. The distinction between them lies in both composition and reaction mechanisms, as depicted in Figure 2.1. AAMs may include calcium-rich precursors, whereas geopolymers represent the low-calcium end of the alkaline activation spectrum.

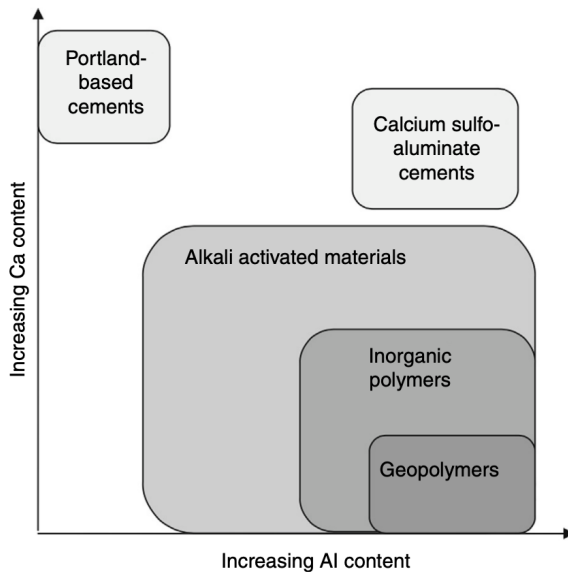
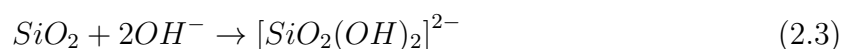
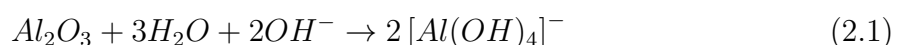


FIGURE 2.1 – Classification of different subsets of alkali-activated materials, with comparisons to Portland cement and calcium sulfoaluminate binder chemistry. Shading indicates approximate alkali content; darker shading corresponds to higher concentrations of Na and/or K (RAKHIMOVA; RAKHIMOV, 2019a).

2.2 Raw Materials for AAM

2.2.1 Precursors

Precursors are materials rich in SiO_2 and Al_2O_3 that, when activated by an alkaline solution, form a three-dimensional network of aluminosilicates (RAKHIMOVA; RAKHIMOV, 2019b). The mechanical and kinetic properties of AAMs are strongly influenced by the SiO_2/Al_2O_3 ratio (PROVIS, 2007). The initial activation process involves the dissolution of aluminosilicates through the breaking of covalent bonds $Si - O - Si$ and $Al - O - Al$ in a high pH environment (SEVERO *et al.*, 2013). Hydrolysis can be represented as follows:



Subsequently, the dissolved silicates and aluminates react with each other, forming a gel that undergoes polymerization and hardening processes, as illustrated in Figure 2.2.

Precursors can be divided into two categories: those with high calcium content, such

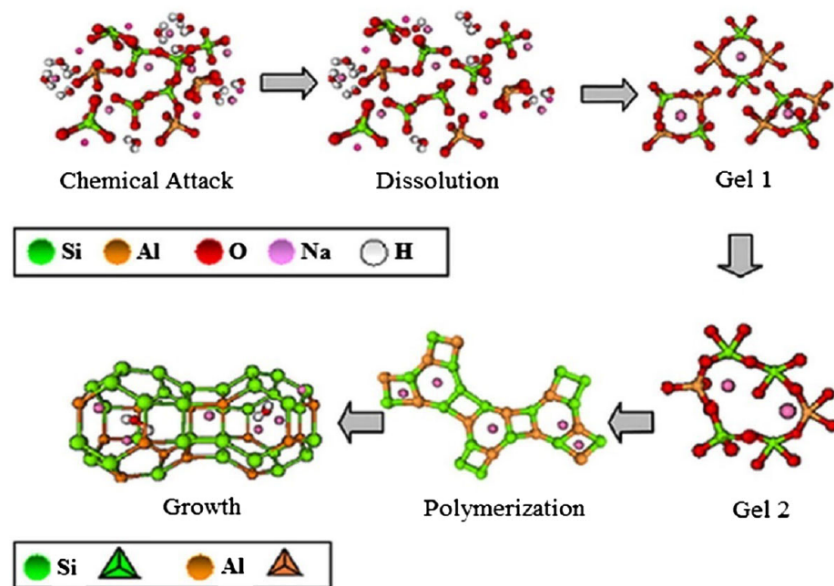


FIGURE 2.2 – Scheme of the alkaline activation process (DUXSON A. FERNÁNDEZ-JIMÉNEZ, 2006).

as blast furnace slag and fly ash, and those with low calcium content, such as metakaolin. Figure 2.3 shows the most common precursors and their respective chemical compositions.

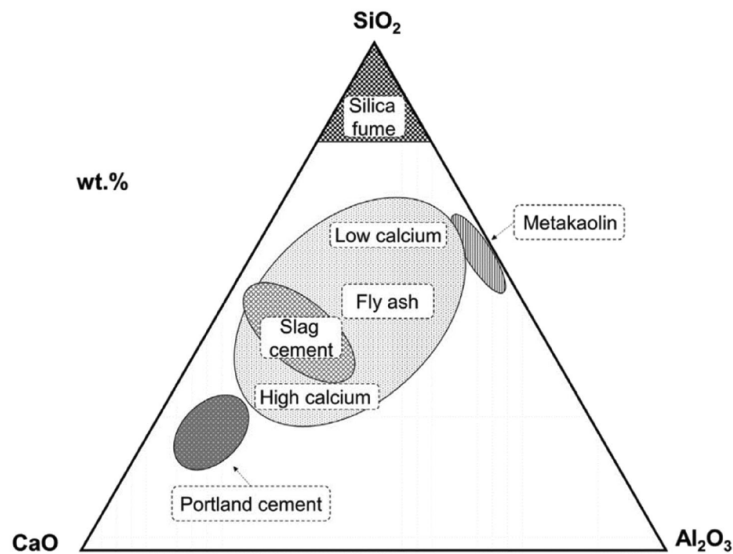


FIGURE 2.3 – Ternary diagram of the most common precursors (GIERGICZNY, 2019).

The first group primarily produces calcium aluminate silicate hydrate (C-A-S-H) as a result of the activation reaction, while the second group predominantly forms sodium aluminosilicate hydrate (N-A-S-H) gel.

When the calcium levels in these precursors are high, the final product is a gel with rapid curing and high initial strength. However, these systems are more susceptible to shrinkage, cracking, and corrosion due to chloride attack. On the other hand, low-calcium systems form an tetrahedral amorphous network, which exhibits low permeability and

shrinkage, better fire resistance, and a less porous structure. The SiO_2/Al_2O_3 ratio is responsible for the degree of polymerization of the formed gel; therefore, if the ideal ratio is not achieved, the mechanical strength and durability of the AAM may be compromised. Finally, the N-A-S-H gel requires a longer curing time and a temperature between 80 – 100 °C to reach the appropriate mechanical strength (NODEHI; TAGHVAEE, 2022).

Table 2.1 presents the main characteristics of the most common precursors.

TABLE 2.1 – Characteristics of common or innovative residual materials that can be added to concrete to produce more sustainable binders (NODEHI; TAGHVAEE, 2022).

Additive name	Usual form	Average density (kg/m ³)	Average particle size (µm)	Limitations	Benefits
Portland cement (OPC)	Irregular and angular	1440	0.15–20	—	—
Silica fume	Spherical	2200	0.1–0.5	Reduces workability and initial strength	Increases compactness, mechanical strength, and durability
Ground granulated blast furnace slag (GGBFS)	Angular with rough surface	1000–1300	1.25–250	Low initial strength	Increases durability, improves ITZ, and sulfate resistance
Fly ash	Spherical	540–860	0.5–300	Low initial strength	Improves workability and long-term strength
Metakaolin	Porous, lamellar, and angular	890	1–20	Reduces workability	Fills microstructure and improves ITZ
Rice husk ash	Irregular with high porosity	504–700	5–10	Property variation and low reactivity	High silica content; improves compactness and strength
Glass powder	Irregular	2500	0.8–50	High contamination	Improves durability and pozzolanic reaction
Red mud	Irregular and needle-shaped	2700–3400	100 to over 200	High contamination	High alumina content, can improve hydration
Ceramic waste	Angular	1700	Below 100	—	Improves compactness and performance
Municipal waste incineration slag (MSWI)	Irregular	660–1690	—	—	Improves microstructure and reduces porosity
Paper sludge ash	Irregular	Below 100	—	—	Favourably adjusts the S/A ratio

2.2.2 Activators

The alkaline attack on the microstructure of the precursors results in the release of silicates and aluminates into the solution. The solubility of silica and alumina as a function of pH is presented in Figure 2.4.

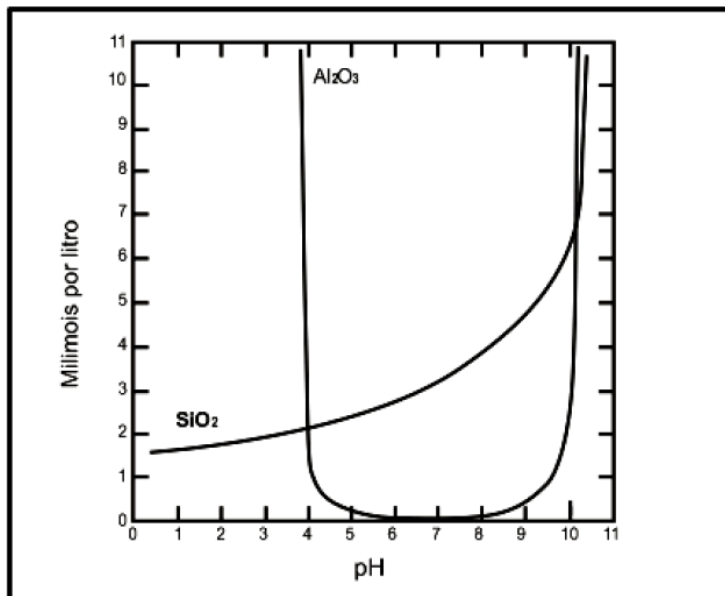


FIGURE 2.4 – Solubility of silica and alumina as a function of pH (MASON, 1952).

It is observed that the solubility of silica is low in acidic environments and high in basic media, while alumina is soluble at both extremes of pH. Therefore, for the activation reactions to occur, it is necessary that the pH of the solution is high.

Alkaline activators can be found in two forms: liquid—producing two-part geopolymers—or solid—one-part geopolymers. The main liquid alkaline activators are: sodium hydroxide ($NaOH$), sodium silicate (Na_2SiO_3), potassium hydroxide (KOH), sodium carbonate (Na_2CO_3), potassium carbonate (K_2CO_3), and potassium oxide (K_2O). The first studies on AAM focused on liquid activators, since the final product exhibits high compressive strength, adhesion, and the ability to withstand fatigue loads. In addition, they also demonstrate high resistance to freeze-thaw cycles and high temperatures (HEATH *et al.*, 2014).

Despite the advantages of two-part systems, basic solutions are corrosive and irritate human skin, making their transport and handling hazardous for workers (AWOYERA, 2019). Another point worth noting is that the production of sodium silicate occurs between 1200 – 1400 °C and emits approximately 1.514 kg of CO_2 per kg of silicate produced, in addition to significantly contributing to air pollution through dust and nitrogen and sulfur oxides (RAJAN, 2020).

Thus, one-part systems emerge as a safer alternative, since solid activators are less

hazardous and easier to handle. Even though one-part geopolymers exhibit lower mechanical strength and require thermal curing to achieve adequate performance (PROVIS, 2018), their use is more scalable.

2.3 Environmental Impacts

The main environmental advantage attributed to AAMs lies in the considerable reduction of CO_2 emissions compared to traditional Portland cement. It is estimated that the environmental impacts of solid and liquid activators are 24% and 60% of the impact caused by OPC, respectively (LUUKKNEN Z. ABDOLLAHNEJAD, 2017). Furthermore, the production of AAMs often utilizes industrial residues as raw materials, such as blast furnace slag, sewage sludge ash, rice husk ash, sugarcane straw ash, among others (MORAES *et al.*, 2024). Therefore, in addition to the valorization of industrial waste, the production of AAMs reduces the demand for natural resources from mineral deposits and provides an environmentally appropriate destination, following the guidelines of the National Solid Waste Policy (BRASIL, 2016).

2.4 Mechanical Properties

3 Methodology

3.1 Materials

For the development of one-part geopolymeric pastes and mortars, the following components were used:

- Caolin supplied by the company Brasilminas;
- Silica fume (SF) supplied by the company Elken;
- Potassium carbonate supplied by the company Neon (purity of 98%);
- Calcium hydroxide supplied by the company Neon (purity of 95%);
- Standardized quartz sand supplied by the company IPT;
- Distilled water.

The precursors used were silica fume and metakaolin. However, the purity of commercially available metakaolin is not sufficient to ensure precision in the characterization of cementitious samples. Therefore, it was produced from commercial kaolin, as detailed in Section 3.2.1.1. The alkaline sources are commercially available with high purity, so the physicochemical compositions provided by the manufacturer were used.

In addition, the quartz sand used follows the standards established by the Institute for Technological Research (IPT), as shown in Tables 3.1 and 3.2.

TABLE 3.1 – Results of physical and chemical requirements of standardized quartz sand.

Property	Result	ABNT NBR7214:2015 Requirement
Silica content NBR14656:2001)	(ABNT 96.5%	$\geq 95\%$, by mass
Moisture NBR7214:2015)	(ABNT 0.0%	$\leq 0.2\%$, by mass
Organic matter NBR17053:2022)	(ABNT Lighter or equal to the color of the standard solution	Color of the 2% tannic acid standard solution

TABLE 3.2 – Particle size distribution of the fractions of standardized quartz sand.

Fraction	Sieve interval	Mass percentage (%)	
		Result	ABNT NBR7214:2015 Requirement
16	(2.4 mm and 2.0 mm)	0	≤ 10
16	(2.0 mm and 1.2 mm)	97	≥ 90
30	(1.2 mm and 0.6 mm)	99	≥ 95
50	(0.6 mm and 0.3 mm)	96	≥ 95
100	(0.3 mm and 0.15 mm)	95	≥ 95

3.2 Methods

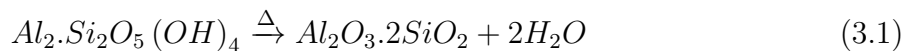
The experimental process was divided into three steps: (i) production and characterization of raw-materials; (ii) production of geopolymeric pastes and mortars; (iii) microstructural studies and mechanical tests of hardened state.

3.2.1 Production and Characterization of Raw Materials

3.2.1.1 Production of Metakaolin

Metakaolin was obtained by calcining kaolin at 700 °C for 1 hour in a 200 L 18 kW laboratory furnace. The optimal calcination time and temperature were determined from preliminary tests, in which the yield of calcination and reactivity was evaluated. To ensure material homogeneity, two shallow trays with a maximum height of 10 mm were used.

The transformation of crystalline kaolinite into amorphous metakaolinite is represented by Equation 3.1.



3.2.1.2 Physicochemical Characterization of Solid Precursors

The physicochemical characterization of the solid precursors was carried out at the laboratories of the Aeronautics Institute of Technology (ITA), located in São José dos Campos-SP.

The removal of hydroxyl groups (OH^-) was verified by loss on ignition (LOI). In addition, X-ray diffraction (XRD) was used to verify the absence of crystalline phases of metakaolin and silica fume, as they are amorphous. XRD was performed by a Panalytical Empyrean diffractometer, with a 2θ interval of 10-70°, Cu-K α radiation, 0.01° step and 50 s/step.

Furthermore, the oxide compositions of metakaolin and silica fume were determined by X-ray Fluorescence (XRF). The results were used to calculate the Si/Al molar ratios and to verify the purity of the precursors. Energy-dispersive X-ray spectroscopy (EDS) was performed together with scanning electron microscopy (SEM) to evaluate the morphology of the solid precursors. SEM/EDS was conducted using a TESCAN VEGA 3 XMU device and Oxford EDS 133 eV detector, with gold coated.

Finally, the particle size distribution (PSD) of the solids used was determined by laser diffraction. Smaller and more irregular particles tend to have a higher specific surface area and, therefore, greater reactivity in contact with the alkaline source, which can directly influence the mechanical performance and rheological properties of the geopolymeric mortars. PSD was analyzed in a Malvern Mastersizer 3000 particle size analyzer, with air as the dispersion agent, at 1.5 bar pressure and a 40% feed rate.

3.2.2 Production of Geopolymeric Pastes and Mortars

3.2.2.1 Mix Design

The development of one-part geopolymeric mortars followed a systematic experimental design, aiming to evaluate the effect of different compositions on physicochemical and mechanical properties.

The variables considered in the study were:

- Proportion between solid precursors (metakaolin and silica fume);

- Content of alkaline activators (K_2CO_3 and $Ca(OH)_2$);
- Water/solids ratio (w/s);
- Sand/binder ratio (s/b).

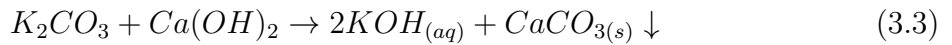
The variable of interest in this experiment is the Si/Al ratio, which will be varied from 1.0 to 5.0, calculated based on the proportion of metakaolin and silica fume.

Initially, the water-to-solids ratio was determined to ensure adequate workability of the pastes, targeting a spread diameter of 200–250 mm in the mini-slump test.

In addition, due to stoichiometric balance, the Al/K ratio will be constant and equal to 1, according to the empirical formula on Equation 3.2 (DAVIDOVITS, 1991), where M is a sodium or potassium cation.

$$M_n \{ (SiO_2)_z AlO_2 \}_n \cdot wH_2O \quad (3.2)$$

Furthermore, the K/Ca ratio will be constant and equal to 2, respecting the precipitation reaction of potassium carbonate with calcium hydroxide, as shown in Equation 3.3.



With the paste proportions well defined, the production of mortars maintained a 1:2 ratio between binder and sand, analogously in the previous researches (BATISTA *et al.*, 2025).

3.2.2.2 Mixing Procedure

The production of the mixtures followed standardized procedures. For the production of mortars and compressive strength testing, the procedures of the Brazilian standard (ABNT, 2019) were followed. For the production of pastes, the American standard (ASTM, 2006) was chosen, since the Brazilian standard does not specify the mixing procedure for cementitious pastes without fine aggregate. Both procedures were adapted for the preparation of small-volume samples.

3.2.2.3 Molding and Curing of Specimens

For the compressive strength test, the specimens were prepared in prismatic molds with dimensions $40 \times 40 \times 40$ mm, previously lubricated with oil-based release agent.

For each composition, 9 specimens were molded, intended for testing at ages of 1, 3, and 7 days (3 specimens for each age). It was not necessary to perform tests at 28 days, as the thermal curing of the binders used provides high initial strength gain.

Thermal curing was carried out in an oven maintained at $(60 \pm 2)^\circ\text{C}$ and a minimum relative humidity of 95% for 24 hours, as recommended by the standard (ABNT, 2006), to ensure the activation of the binders and accelerate the curing process. It is noteworthy that demolding was performed 24 hours after the start of the curing process. After demolding, the specimens were immediately transferred to the corresponding curing conditions until the testing age.

For microstructural analyses, small samples were separated, with hydration interrupted by immersion in ethyl alcohol and vacuum filtration, followed by drying in an oven at 40°C for 24 hours. These samples were stored in hermetically sealed containers to prevent rehydration.

3.2.3 Microstructural studies and Mechanical tests of hardened state

3.2.3.1 Characterization of Geopolymeric pastes

The microstructural characterization of the hardened pastes was performed by X-ray diffraction (XRD), Fourier-transform infrared spectroscopy (FTIR), scanning electron microscopy (SEM) with energy-dispersive X-ray spectroscopy (EDS), and mercury intrusion porosimetry (MIP).

To verify the presence of $\text{Al} - \text{Si} - \text{O}$ bonds, Fourier-transform infrared spectroscopy (FTIR) was carried out in a PerkinElmer spectrophotometer, with a spectrum range of $4000\text{--}400 \text{ cm}^{-1}$ and a spectral resolution of 1 cm^{-1} . Moreover, XRD, SEM/EDS PSD were performed under the same conditions applied for the raw materials. Lastly, the total porosity and pore size distribution of the hardened pastes were determined by mercury intrusion porosimetry (MIP).

3.2.3.2 Compressive Strength of mortars

For the compressive strength test, the specimens were placed in a hydraulic press with a 600 kN-load limit, applying load at a rate of 0.5 kN/s until failure. The strength was calculated by the equation:

$$R_c = \frac{F_c}{A_t} \quad (3.4)$$

Where:

- R_c is the compressive strength, in MPa;
- F_c is the maximum applied load, in N;
- A_t is the cross-sectional area, in mm².

For statistical analysis, the Tukey test was performed, allowing the identification of significant differences between sample groups, considering a significance level of 95%. The Table reftab:methods summary presents the summary of the methods used in this work.

4 Results and Discussion

4.1 Chemical and Physical Characterization of Precursors

4.1.1 Chemical Composition of Precursors

The chemical composition of the aluminosilicate precursors plays a fundamental role in determining their reactivity and suitability for activation in a low-calcium system. In this work, the metakaolin (MK) and active silica (SA) precursors were analysed for their oxide content (normalized with respect to the powder fraction) and loss on ignition (LOI), which was found to be 0.69% and 2.27%, respectively.

TABLE 4.1 – Chemical composition (wt %) of the precursors: metakaolin (MK) and active silica (SA).

Oxide	Metakaolin		Active Silica	
	wt (%)	wt with LOI (%)	wt (%)	wt with LOI (%)
K ₂ O	0.21	0.20	0.74	0.73
CaO	0.19	0.19	0.13	0.13
MgO	2.60	2.59	0.00	0.00
P ₂ O ₅	0.00	0.00	0.00	0.00
Cl	0.00	0.00	0.12	0.12
SO ₃	0.00	0.00	0.15	0.15
SiO ₂	49.37	49.03	96.90	94.70
Fe ₂ O ₃	0.77	0.76	1.78	1.74
Al ₂ O ₃	46.38	46.06	0.00	0.00
Na ₂ O	0.00	0.00	0.17	0.17
TiO ₂	0.49	0.48	0.00	0.00

From Table 4.1.1 it is clear that the MK precursor is rich in alumina and contains a significant silica fraction , while the SA is extremely high in silica and essentially alumina-free. Critically, both materials present very low CaO contents. The minimal presence of calcium oxide is an important indicator of the low-calcium nature of the precursors, which is a pre-requisite for favoring the formation of potassium aluminosilicate hydrate

type gels, rather than calcium-rich gels, as often observed when using ground granulated blast furnace slag (ALI *et al.*, 2023).

In addition, the low LOI values suggest a limited amount of residual organics or volatile components, which could otherwise interfere with the dissolution kinetics of the aluminosilicates. Furthermore, the Si/Al molar ratio of MK precursors is approximately 0.9, which will be used with the essentially pure SA to tailor the mix designs for optimal geopolymers reactions, as presented in Appendix A.

In summary, the chemical data confirm that both MK and SA meet the key requirements of (i) high silica and/or alumina content, (ii) low calcium content, and (iii) minimal impurities, thereby validating their use as raw materials for a low calcium alkali-activated binder system.

4.1.2 X-Ray Diffraction of Precursors and Alkaline Sources

XRD analysis was conducted on the precursors and alkaline sources to evaluate phase composition, crystallinity and the presence of amorphous phases. The key observations were as follows:

TABLE 4.2 – Summary of XRD phase observations for precursors and alkaline sources.

Material	Key XRD observations
MK	Broad amorphous hump near $2\theta \approx 21^\circ$, residual quartz peaks (COD 900-9667)
SA	Broad amorphous hump near $2\theta \approx 22.5^\circ$, no distinct crystalline phases
$\text{Ca}(\text{OH})_2$	Crystalline portlandite phase (COD 900-0114)
K_2CO_3	Crystalline calcium carbonate phase (COD 900-9644)

SA and MK both exhibited broad amorphous humps in their XRD patterns, indicative of their largely non-crystalline nature, which is favorable for dissolution during alkali activation. The MK showed minor crystalline quartz peaks, indicating the presence of impurities, which remains inert during calcination (PROVIS; BERNAL, 2014) and acts as filler without participating in geopolymers reaction (RAKHIMOVA; RAKHIMOV, 2019b). The alkaline sources displayed sharp diffraction peaks corresponding to their known crystalline phases, confirming their purity.

4.2 Microstructural Characterization of Pastes

4.2.1 Scanning Electron Microscopy and Energy Dispersive Spectroscopy

Scanning electron microscopy of the pastes cured for 3 days revealed a clear dependence of matrix morphology on the Si/Al molar ratio. At Si/Al ratio of 0.9, the SEM images of the paste showed a higher frequency of visibly unreacted precursor particles, together with needle-shaped crystalline features and larger pores. Those unreacted particles are likely some alkali carbonate products that precipitate when mobile alkalis are not fully incorporated into the aluminosilicate gel and subsequently react with atmospheric CO₂ (PROVIS, 2018).

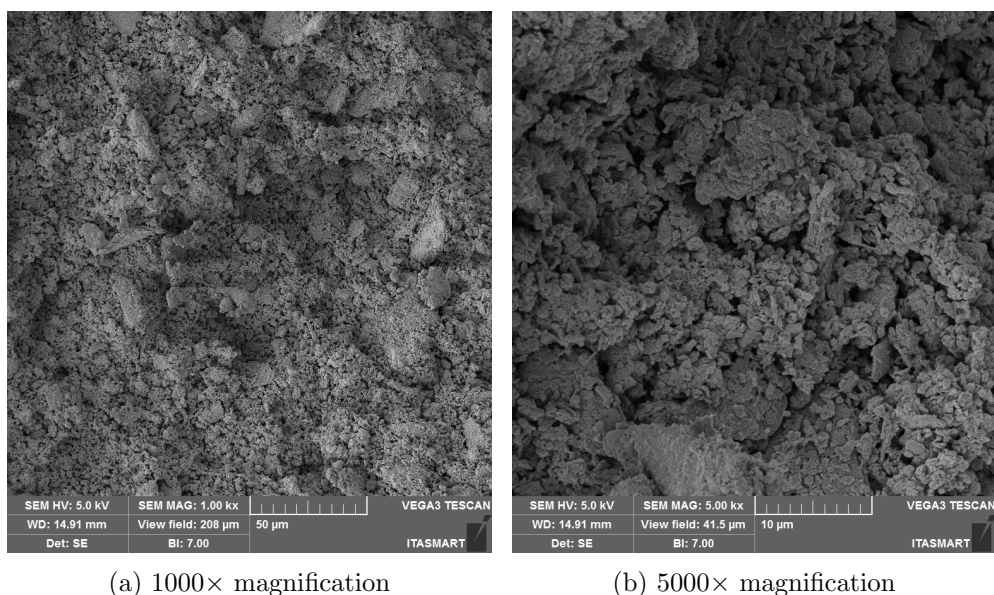


FIGURE 4.1 – SEM micrographs of paste with Si/Al = 0.9 after 3 days of curing (spot 5).

By contrast, the Si/Al ratio of 3.0 paste exhibited the densest and most homogeneous matrix, with fewer discernible unreacted particles and a more continuous binder phase. This indicates that intermediate Si/Al values promote better network polymerization and denser structure.

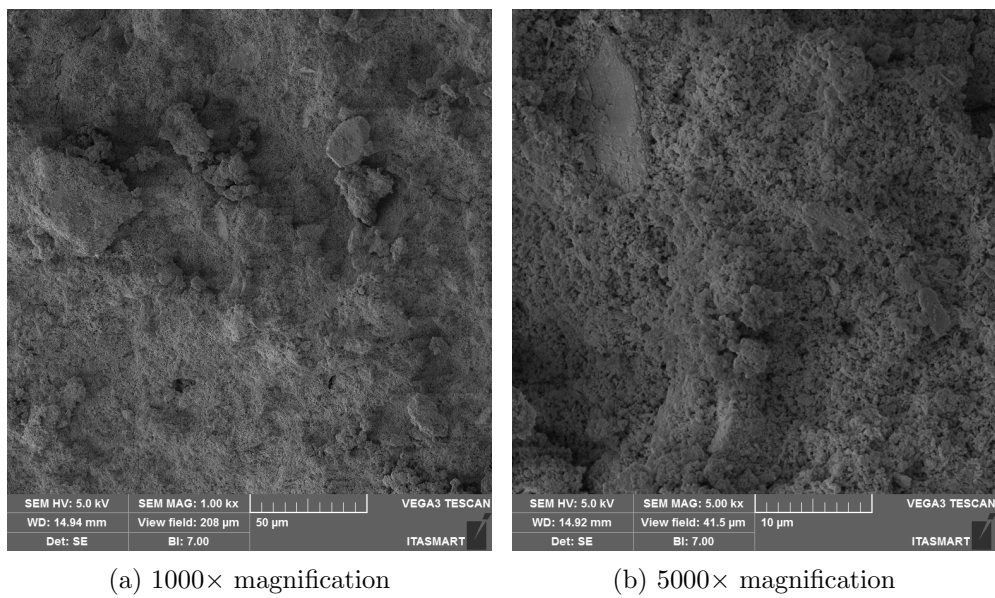


FIGURE 4.2 – SEM micrographs of paste with Si/Al = 3.0 after 3 days of curing (spot 3).

At Si/Al = 5.0, the SEM images showed residual spherical particles characteristic of silica fume that were not fully reacted after the curing time, indicating that at very high Si/Al the silica supply exceeds the polymerization capacity of the system.

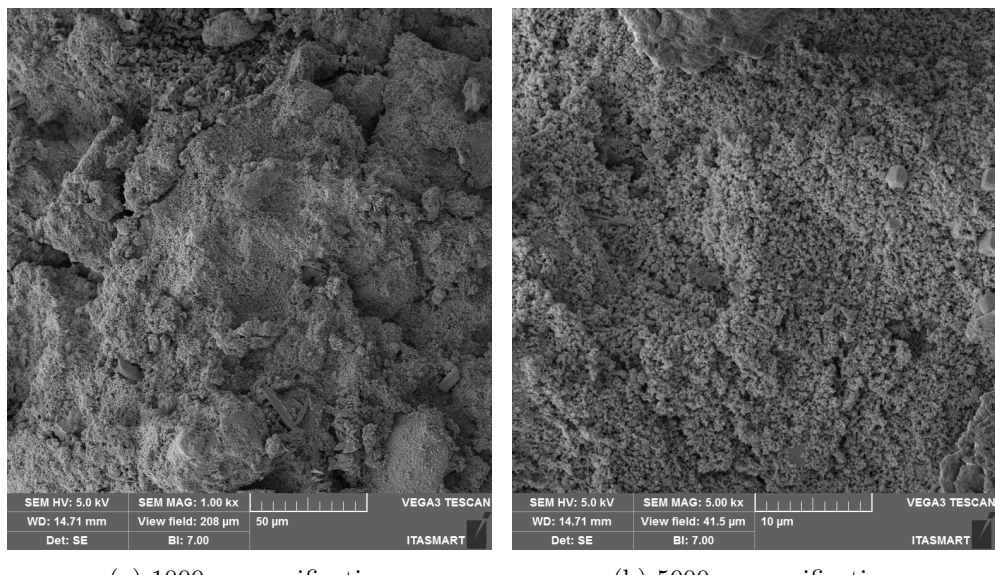


FIGURE 4.2 SEM micrographs of paste with Si/Al = 5.0 after 2 days of curing (spot 1)

The remaining pictures from SEM analysis are presented in Appendix B

Energy dispersive spectroscopy was performed at representative gel regions and crystalline features observed in the SEM images.

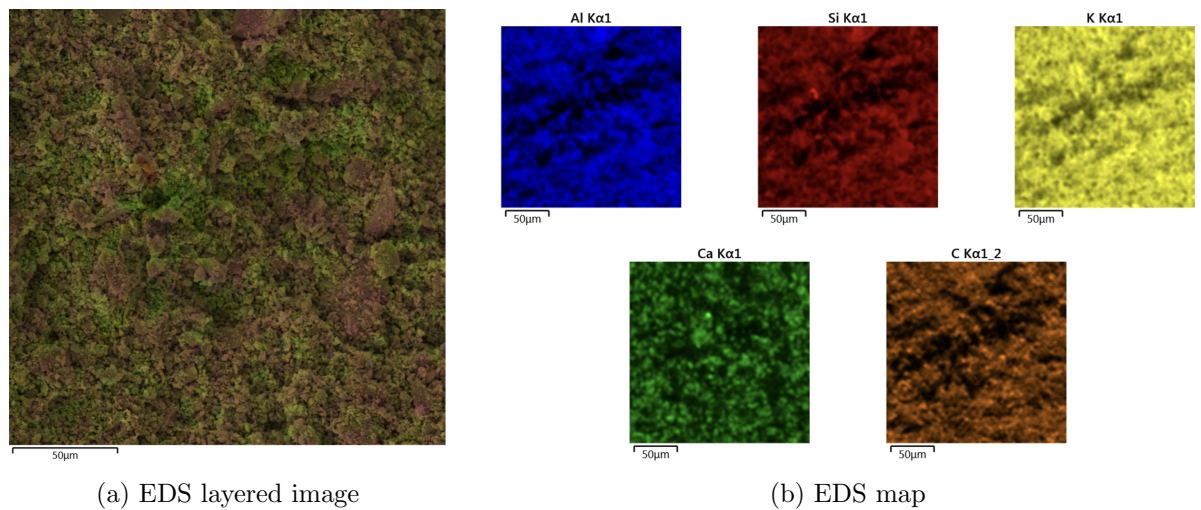


FIGURE 4.4 – EDS analysis of Spot 5, $\text{Si}/\text{Al} = 0.9$, cured for 3 days at 60°C at $1000\times$ magnification.

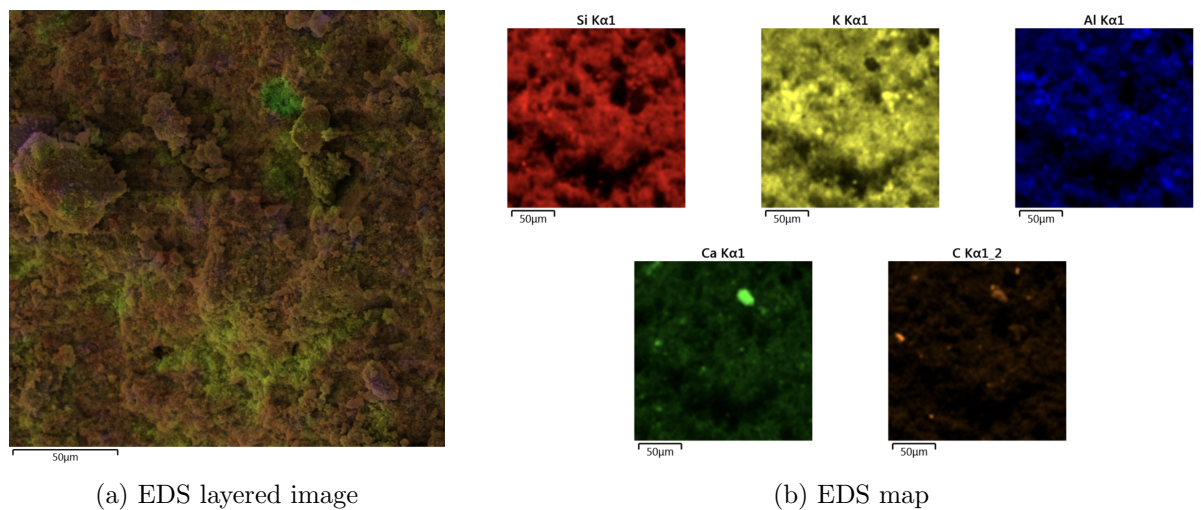


FIGURE 4.5 – EDS analysis of Spot 3, $\text{Si}/\text{Al} = 3.0$, cured for 3 days at 60°C at $1000\times$ magnification.

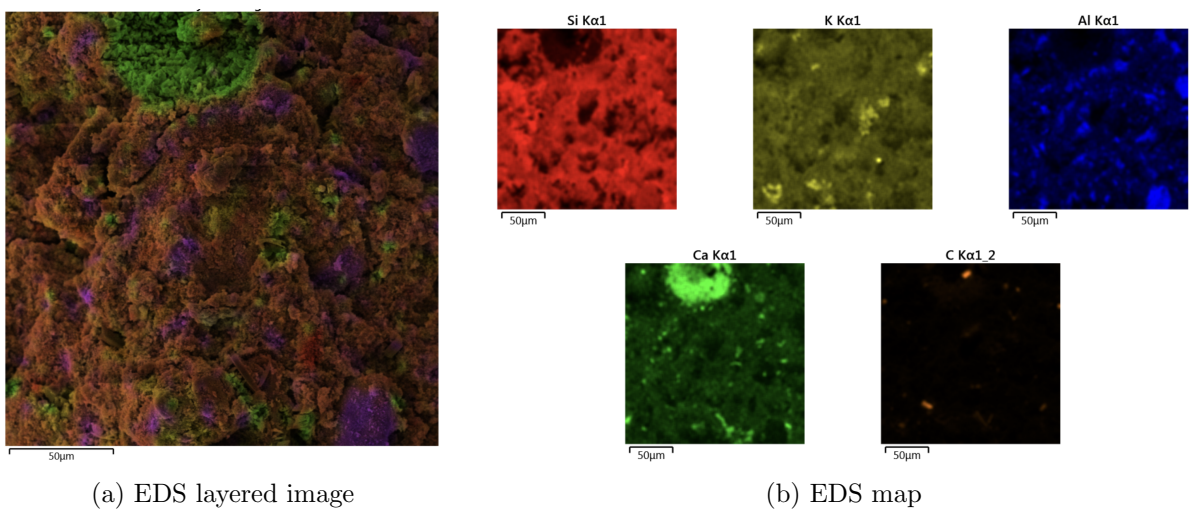


FIGURE 4.6 – EDS analysis of Spot 1, Si/Al = 5.0, cured for 3 days at 60°C at 1000 \times magnification.

The spectrum results are summarized in Table 4.3 and it can be noted that the K/Ca ratio was approximately constant and equals to 2, as expected from the mix design. However, the Si/Al ratio from EDS was slightly higher than the intended mix design values. It can be speculated that this is due to a stronger tendency of Si to stay in solution rather than being incorporated into the gel structure and precipitate during geopolymmerization at high pH environment (CHEN *et al.*, 2024). **Am I missing something?**

TABLE 4.3 – EDS spectrum of pastes after 3 days of curing at 60°C.

Sample	At(%)				Wt(%)			
	Si	Al	K	Ca	Si	Al	K	Ca
0.9_60C_3d_Spot5	26.4	27.1	30.4	16.0	22.4	22.1	36.0	19.5
3.0_60C_3d_Spot3	54.2	13.5	21.5	10.8	48.2	11.5	26.6	13.7
5.0_60C_3d_Spot1	59.5	9.2	19.6	11.6	53.0	7.9	24.2	14.9

Additional EDS spectral data for all analyzed spots can be found in Appendix C.

4.2.2 X-Ray Diffraction

X-ray diffraction patterns (3-day curing) of the pastes at different Si/Al ratios showed a persistent amorphous hump in all compositions, indicating the presence of aluminosilicate gel (N-A-S-H). The hump position and shape were increasingly similar to the active silica precursor at high Si/Al, consistent with the SEM observation, as it shifted to the left as silica content increases.

In agreement with other studies, the geopolymization process—which is responsible for the strength—is indicated by the presence of the broad hump among $2\theta = 20 \approx 35^\circ$.

process shifted the location of the amorphous hump to lower angles as the silica proportion increases (ARELLANO-AGUILAR *et al.*, 2014; LEE *et al.*, 2017; WAN *et al.*, 2017).

The patterns of the pastes show sharp peaks of crystalline phases of solid precursors, this indicates that they were not involved in the geopolymerization process (GERALDO, 2020), but were rather present as inactive fillers, as noted by (RUIZ-SANTAQUITERIA *et al.*, 2012). The crystalline phases identified in the XRD patterns are presented in Table 4.4, showing the semi-quantitative phase composition at 3 days for different Si/Al ratios.

TABLE 4.4 – Semi-quantitative crystalline phases at 3 days for different Si/Al ratios (XRD).

Phase (%)	Si/Al				
	0.9	2.0	3.0	4.0	5.0
Calcite (CaCO_3)	77	56	43	52	79
Butschliite ($\text{K}_2\text{Ca}(\text{CO}_3)_2$)	18	29	0	0	0
Aragonite (CaCO_3)	0	0	41	24	0
Quartz (SiO_2)	6	14	16	17	21
Stishovite (SiO_2)	0	0	0	7	0

Figure 4.7 exhibits that at lower Si/Al ratios, the peaks - specially from calcite - are more intense, indicating a higher presence of these crystalline phases from unreacted materials.

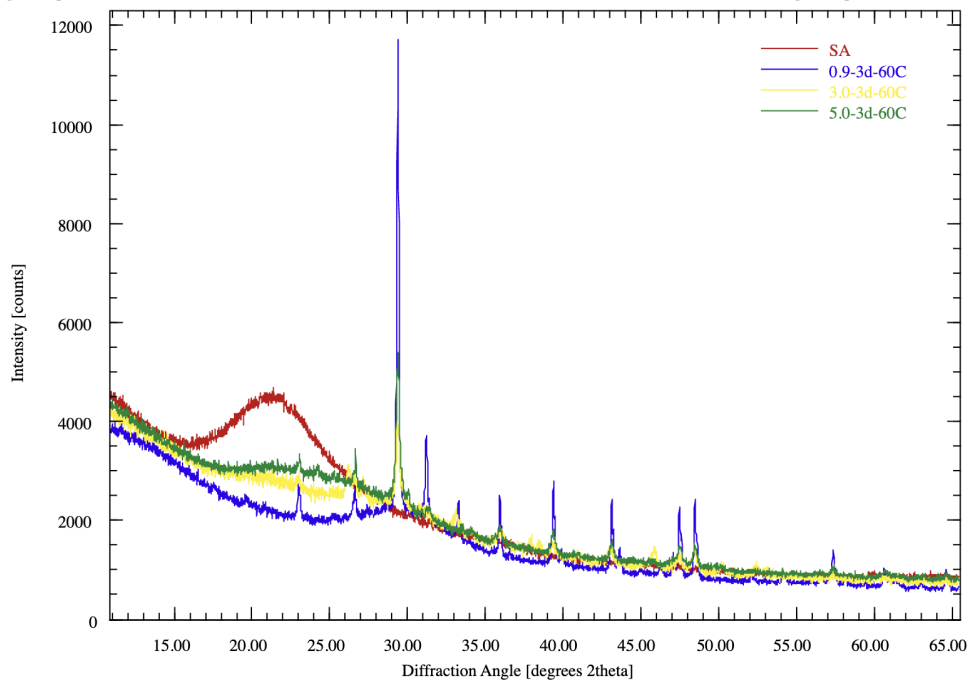


FIGURE 4.7 – XRD patterns of pastes at different Si/Al ratios after 3 days of curing.

Find a better way to present this graph, shifting vertically different ratios and labeling

the peaks.

4.2.3 Fourier Transform Infrared Spectroscopy

FTIR spectra were collected for all pastes after 1 and 3 days of curing to analyze the chemical bonding and structural changes associated with geopolymers at different Si/Al ratios. There was no significant variation in the spectra from 1 to 3 days of curing, so only the spectra after 3 days are represented in Figure 4.8. The spectra of solid precursors are exhibited in Appendix D.

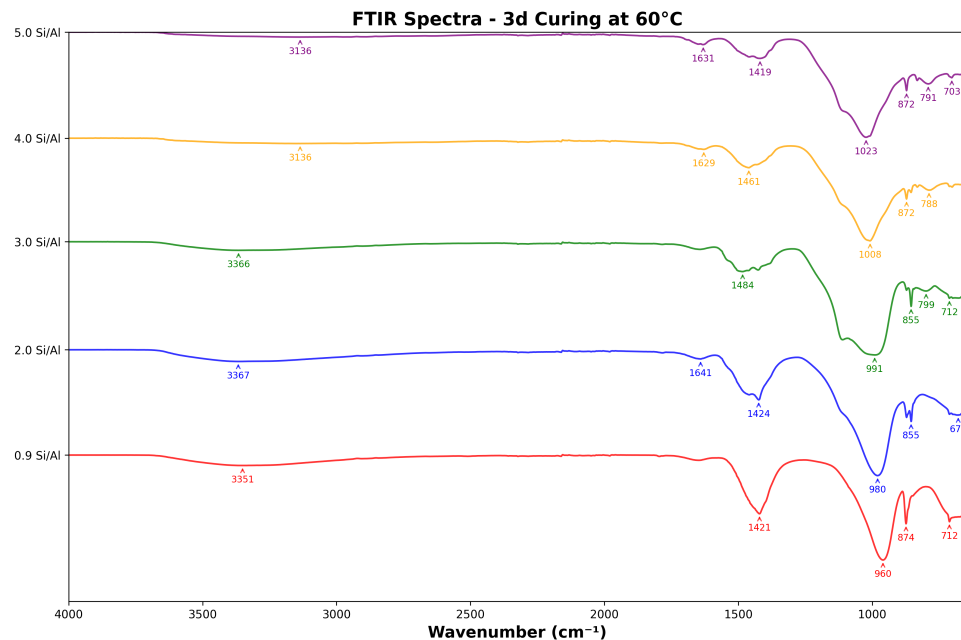


FIGURE 4.8 – FTIR spectra of pastes at different Si/Al ratios after 3 days of curing.

The key to interpreting these spectra lies in the fingerprint region ($400\text{-}1200\text{ cm}^{-1}$), which reflects the formation of the polymeric network, and the hydroxyl/carbonate regions ($1300\text{-}3700\text{ cm}^{-1}$), which indicate water and carbonation. The Table 4.5 summarizes the main FTIR peaks observed in the pastes and their assignments.

TABLE 4.5 – Assignment of FTIR absorption bands observed in pastes after 3 days of curing at 60°C, where T = Si or Al.

Wavenumber Range (cm ⁻¹)	Observed Peaks	Vibration Mode	Chemical Significance	Reference
3100-3450	3111, 3136, 3177, 3325, 3367	O-H stretching	Represents weakly bonded or physically adsorbed water, and hydroxyl groups involved in hydrogen bonding within the gel structure.	(ZHAO et al., 2023), (PRO-VIS; DEVENTER, 2009), (MA et al., 2022)
1620-1645	1629, 1631, 1632, 1641	H-O-H bending	Vibration of interlayered or physically bound water molecules in the AAM matrix.	(ZHAO et al., 2023), (PACHECO-TORGAL et al., 2014)
1350-1500	1419, 1423, 1461, 1484	C-O stretching	Characteristic of carbonates, indicating atmospheric carbonation (formation of CaCO ₃ or K ₂ CO ₃).	(ZHAO et al., 2023), (PACHECO-TORGAL et al., 2014), (MORAES et al., 2024)
950-1100	960, 1008, 1023	Si-O-T asymmetric stretching	Primary diagnostic band of N-A-S-H gel formation. Shifted to lower frequencies when compared to precursors (SA: 1040, MK: 1051 cm ⁻¹) indicates precursor dissolution and gel polymerization.	(MA et al., 2022), (ZHAO et al., 2023), (PRO-VIS; DEVENTER, 2009)
780-880	787, 855, 872	Si-O-Si symmetric stretching or C-O bending	Peaks around 780-800 cm ⁻¹ relate to unreacted quartz. Bands in 850-880 cm ⁻¹ are associated with carbonate bending vibrations.	(MORAES et al., 2024), (PACHECO-TORGAL et al., 2014)
550-700	563, 679, 703, 712	O-T-O or Al-O-T bending	Associated with bending vibrations in the tetrahedral network, specifically Al-O linkages in AlO ₄ units or O-Si-O bending.	(ZHAO et al., 2023), (MA et al., 2022)

5 Conclusion

Lorem ipsum dolor sit amet, consectetur adipiscing elit. Nullam venenatis augue id augue ultrices, et gravida magna vehicula. Cras volutpat suscipit iaculis. Praesent varius ac orci sed ultrices. Vivamus vestibulum molestie lorem. Maecenas id congue tortor. Aliquam erat volutpat. Nullam ornare tortor et nunc sagittis laoreet. Sed at turpis et quam facilisis elementum. Nullam ultrices elit ut accumsan ultricies. Nulla sit amet tellus lacus. Vestibulum ac lectus velit. Donec nunc odio, mattis nec orci sed, porta lobortis lectus.

Proin ultricies elit vitae mi efficitur eleifend. Nulla non lorem consectetur, placerat dui quis, feugiat urna. Quisque sed ligula massa. Donec finibus placerat orci, eget mollis justo rutrum a. Sed luctus feugiat congue. Phasellus libero felis, tempor quis rutrum pretium, porttitor ac nisi. Praesent euismod malesuada enim a rhoncus. Aliquam gravida fringilla aliquam. Proin nunc lorem, convallis fringilla eleifend et, tempus quis orci. Phasellus bibendum, tellus eu elementum posuere, odio lacus maximus eros, nec lobortis lectus nisi a turpis. Vivamus viverra felis et dolor viverra interdum. Nulla convallis nisi eu sapien egestas aliquet sit amet eget risus. Phasellus vel quam vel lacus commodo lacinia.

Donec ultrices ac nisi nec elementum. Aenean pellentesque pellentesque pulvinar. Ut aliquet nulla vitae porttitor hendrerit. Nullam venenatis nisl nec ipsum malesuada ultricies. Curabitur massa erat, auctor in ipsum non, semper ornare nunc. Donec non felis eget diam porta rhoncus. Mauris id lectus sed arcu iaculis dictum et vitae velit. Cras sit amet neque vel sapien interdum fermentum sit amet eu lorem. Fusce urna sem, pretium a facilisis id, aliquet at mi. Etiam elementum eget est et porttitor. Morbi ultricies lorem a arcu mattis, eget egestas ex ultrices. Pellentesque bibendum sed est ac imperdiet.

Bibliography

ABNT. ABNT NBR 9479:2006 - Argamassa e concreto — Câmara úmidas e tanques para cura de corpos-de-prova. 2. ed. Rio de Janeiro, Brasil, maio 2006. Válida a partir de 30 de junho de 2006.

ABNT. ABNT NBR 7215: Cimento Portland — Determinação da resistência à compressão de corpos de prova cilíndricos. Rio de Janeiro, Brasil, 2019. Segunda edição. Publicada em 28/02/2019.

ALI, S. A.; TAHIR, M. F.; REHMAN, S.; SIDDIQUE, R.; RANA, M. A.; FAROOQ, M.; KHAN, W. A. Geopolymer chemistry and composition: A comprehensive review of synthesis, reaction mechanisms, and material properties—oriented with sustainable construction. **Case Studies in Construction Materials**, Elsevier, v. 19, p. e02089, 2023.

ANDREW, R. M. Global co₂ emissions from cement production. **Earth System Science Data**, Copernicus GmbH, v. 10, n. 1, p. 195–217, 2018.

ARELLANO-AGUILAR, R.; BURCIAGA-DÍAZ, O.; GOROKHOVSKY, A.; ESCALANTE-GARCÍA, J. I. Geopolymer mortars based on a low grade metakaolin: Effects of the chemical composition, temperature and aggregate: binder ratio. **Construction and Building Materials**, Elsevier, v. 50, p. 642–648, 2014.

ASTM. ASTM C305: Standard Practice for Mechanical Mixing of Hydraulic Cement Pastes and Mortars of Plastic Consistency. West Conshohocken, PA, USA, 2006. Designação oficial: ASTM C305-06.

AWOYERA, A. A. P. O. A critical review on application of alkali activated slag as a sustainable composite binder. **Miscellaneous**, v. 11, p. e00268–e00268, 2019.

BATISTA, J.; CORDEIRO, G.; RIBEIRO, L.; MORAES, J. Improved microstructure and compressive strength of pastes and mortars containing mgo–sio₂ cement produced by combined calcination of mgco₃ and kaolin. **Cement and Concrete Composites**, v. 157, p. 105959, 2025.

BERNAL, S. A.; GUTIÉRREZ, R. M. de; PROVIS, J. L. Engineering and durability properties of alkali-activated slag concretes. **Construction and Building Materials**, Elsevier, v. 33, p. 99–108, 2014.

BRASIL. **Política Nacional de Resíduos Sólidos: Lei nº 12.305, de 2 de agosto de 2010, e legislação correlata**. 3. ed. Brasília, 2016. (Série Legislação, n. 230). Atualizada até 12 de fevereiro de 2016.

- CHEN, Y.; LIMA, L. M. de; LI, Z.; MA, B.; LOTHENBACH, B.; YIN, S.; YU, Q.; YE, G. Synthesis, solubility and thermodynamic properties of nash gels with various target si/al ratios. **Cement and Concrete Research**, Elsevier, v. 180, p. 107484, 2024.
- DAVIDOVITS, J. Geopolymers: Inorganic polymeric new materials. **Journal of Thermal Analysis and Calorimetry**, v. 37, p. 1633–1656, 08 1991.
- DUXSON A. FERNÁNDEZ-JIMÉNEZ, J. L. P. P. Geopolymer technology: the current state of the art. **EBSCOhost Academic Search Premier**, v. 42, n. 9, p. 2917–2933, 2006.
- GERALDO, R. H. **Aglomerante álcali-ativado de parte única: obtenção, composição, propriedades e durabilidade**. Thesis (Tese de Doutorado) — Universidade Estadual de Campinas, Campinas, Brasil, 2020. Orientadora: Profa. Dra. Gladis Camarini.
- GIERGICZNY, Z. Fly ash and slag. **Cement and Concrete Research**, v. 124, p. 105826, 2019. ISSN 0008-8846.
- HEATH, A.; PAINE, K.; McMANUS, M. Minimising the global warming potential of clay based geopolymers. **Journal of Cleaner Production**, v. 78, p. 75–83, 2014.
- IEA; WBCSD. **Cement Technology Roadmap 2009: Carbon Emissions Reductions up to 2050**. Paris, France and Geneva, Switzerland, 2009.
- KE, X.; BERNAL, S. A.; PROVIS, J. L. One-part alkali-activated materials: State-of-the-art and perspectives. **Cement and Concrete Research**, Elsevier, v. 140, p. 106336, 2021.
- LEE, B.; KIM, G.; KIM, R.; CHO, B.; LEE, S.; CHON, C.-M. Strength development properties of geopolymer paste and mortar with respect to amorphous si/al ratio of fly ash. **Construction and Building Materials**, Elsevier, v. 151, p. 512–519, 2017.
- LUUKKUNEN Z. ABDOLLAHNEJAD, J. Y. T. One-part alkali-activated materials: A review. **Elsevier ScienceDirect Journals**, v. 103, p. 21–34, 2017.
- MA, B.; LUO, Y.; ZHOU, L.; SHAO, Z.; LIANG, R.; FU, J.; WANG, J.; ZANG, J.; HU, Y.; WANG, L. The influence of calcium hydroxide on the performance of mk-based geopolymer. **Construction and Building Materials**, v. 329, p. 127224, 2022.
- MASON, B. Principles of geochemistry. **Miscellaneous**, v. 74, n. 3, p. 262, 1952.
- MORAES, J.; MORAES, M.; BATISTA, J.; AKASAKI, J.; FONT, A.; TASHIMA, M.; SORIANO, L.; BORRACHERO, M.; PAYÁ, J. Influence of sugar cane straw ash in metakaolin-based geopolymers. **Construction and Building Materials**, v. 444, p. 137835, 2024.
- NODEHI, M.; TAGHVAAE, V. M. Alkali-activated materials and geopolymer: a review of common precursors and activators addressing circular economy. **Circular Economy and Sustainability**, v. 2, p. 165–196, 2022.
- PACHECO-TORGAL, F.; LABRINCHA, J.; LEONELLI, C.; PALOMO, A.; CHINDAPRASIRT, P. (Ed.). **Handbook of Alkali-Activated Cements, Mortars and Concretes**. Oxford, UK: Elsevier, 2014. ISBN 9781782422884.

- PROVIS, J. L. Alkali-activated materials. **Nature Reviews Materials**, Nature Publishing Group, v. 3, n. 6, p. 276–277, 2018.
- PROVIS, J. L.; BERNAL, S. A. Geopolymers and related alkali-activated materials. **Annual Review of Materials Research**, Annual Reviews, v. 44, p. 299–327, 2014.
- PROVIS, J. L.; DEVENTER, J. S. J. van (Ed.). **Geopolymers: Structure, Processing, Properties and Industrial Applications**. Cambridge, UK: Woodhead Publishing / CRC Press, 2009. ISBN 9781845694494.
- PROVIS, J. v. D. J. L. Geopolymerisation kinetics. 1. in situ energy-dispersive x-ray diffractometry. **Elsevier ScienceDirect Journals**, v. 62, n. 9, p. 2309–2317, 2007.
- QIN, Y.; QU, C.; MA, C.; ZHOU, L. One-part alkali-activated materials: State of the art and perspectives. **Polymers**, v. 14, n. 22, p. 5046, 2022.
- RAJAN, P. K. H. S. Sustainable development of geopolymer binder using sodium silicate synthesized from agricultural waste. **Elsevier ScienceDirect Journals**, v. 286, p. 124959–124959, 2020.
- RAKHIMOVA, N. R.; RAKHIMOV, R. Z. Reaction products, structure and properties of alkali-activated metakaolin cements incorporated with supplementary materials—a review. **Journal of Materials Research and Technology**, Elsevier, v. 8, n. 1, p. 1522–1531, 2019.
- RAKHIMOVA, N. R.; RAKHIMOV, R. Z. Reaction products, structure and properties of alkali-activated metakaolin cements incorporated with supplementary materials – a review. **Journal of Materials Research and Technology**, v. 8, n. 1, p. 1522–1531, 2019.
- RUIZ-SANTAQUITERIA, C.; SKIBSTED, J.; FERNÁNDEZ-JIMÉNEZ, A.; PALOMO, A. Alkaline solution/binder ratio as a determining factor in the alkaline activation of aluminosilicates. **Cement and Concrete Research**, Elsevier, v. 42, n. 9, p. 1242–1251, 2012.
- SCRIVENER, K. L.; JOHN, V. M.; GARTNER, E. M. Eco-efficient cements: Potential economically viable solutions for a low-co₂ cement-based materials industry. **Cement and concrete Research**, Elsevier, v. 114, p. 2–26, 2018.
- SEVERO, C. G. S.; COSTA, D. L.; BEZERRA, I. M. T.; MENEZES, R. R.; NEVES, G. A. Características, particularidades e princípios científicos dos materiais ativados alcalinamente. **Revista Eletrônica de Materiais e Processos**, v. 8, n. 2, p. 55–67, 2013.
- United Nations. **World population prospects: The 1994 revision**. [S.l.]: UN, 1995.
- WAN, Q.; RAO, F.; SONG, S.; GARCÍA, R. E.; ESTRELLA, R. M.; PATIÑO, C. L.; ZHANG, Y. Geopolymerization reaction, microstructure and simulation of metakaolin-based geopolymers at extended si/al ratios. **Cement and Concrete Composites**, Elsevier, v. 79, p. 45–52, 2017.
- ZAREECHIAN, M.; SIAD, H.; LACHEMI, M.; SAHMARAN, M. Advancements in cleaner production of one-part geopolymers: A comprehensive review of mechanical properties, durability, and microstructure. **Elsevier ScienceDirect Journals**, v. 409, p. 133876–133876, 2023.

ZHAO, Q.; MA, C.; HUANG, B.; LU, X. Development of alkali activated cementitious material from sewage sludge ash: Two-part and one-part geopolymers. **Journal of Cleaner Production**, v. 384, p. 135547, 2023.

Appendix A - Mix Design Formulations

This appendix presents the detailed mix design formulations for both paste and mortar samples used in this study. The formulations are based on varying Si/Al ratios while maintaining constant Al/K ratio of 1.0 and W/S ratio of 0.45 for all formulations. For the mortar samples, a constant sand-to-binder ratio of 2.0 was maintained to ensure comparable workability and mechanical properties across all mix designs.

TABLE A.1 – Mix design formulations for paste samples with varying Si/Al ratios.

Sample	Alkaline Source	Si/Al	Mass (g)			
			MK	SiO ₂	K ₂ CO ₃ /Ca(OH) ₂	Water
5.0	K ₂ CO ₃ /Ca(OH) ₂	5.0	8.68	20.39	8.59	16.95
4.0	K ₂ CO ₃ /Ca(OH) ₂	4.0	10.02	17.78	9.91	16.97
3.0	K ₂ CO ₃ /Ca(OH) ₂	3.0	11.84	14.23	11.71	17.01
2.0	K ₂ CO ₃ /Ca(OH) ₂	2.0	14.48	9.10	14.32	17.05
0.9	K ₂ CO ₃ /Ca(OH) ₂	0.9	19.15	0.00	18.95	17.14

TABLE A.2 – Mix design formulations for mortar samples with varying Si/Al ratios.

Sample	Source	Si/Al	Mass (g)					
			MK	SiO ₂	K ₂ CO ₃	Ca(OH) ₂	Water	Sand
5.0	K ₂ CO ₃ /Ca(OH) ₂	5.0	88.93	208.82	56.65	31.33	173.58	771.47
4.0	K ₂ CO ₃ /Ca(OH) ₂	4.0	102.55	182.03	65.33	36.13	173.72	772.07
3.0	K ₂ CO ₃ /Ca(OH) ₂	3.0	121.10	145.54	77.15	42.66	173.90	772.90
2.0	K ₂ CO ₃ /Ca(OH) ₂	2.0	147.84	92.94	94.18	52.09	174.17	774.09
0.9	K ₂ CO ₃ /Ca(OH) ₂	0.9	195.09	0.00	124.28	68.73	174.64	776.20

Appendix B - SEM Images

This appendix presents the complete collection of SEM images for all analyzed spots across different Si/Al ratios. All specimens were cured for 3 days at 60°C. Each figure shows four magnifications: 500 \times , 1000 \times , 2500 \times , and 5000 \times .

B.1 Si/Al = 0.9

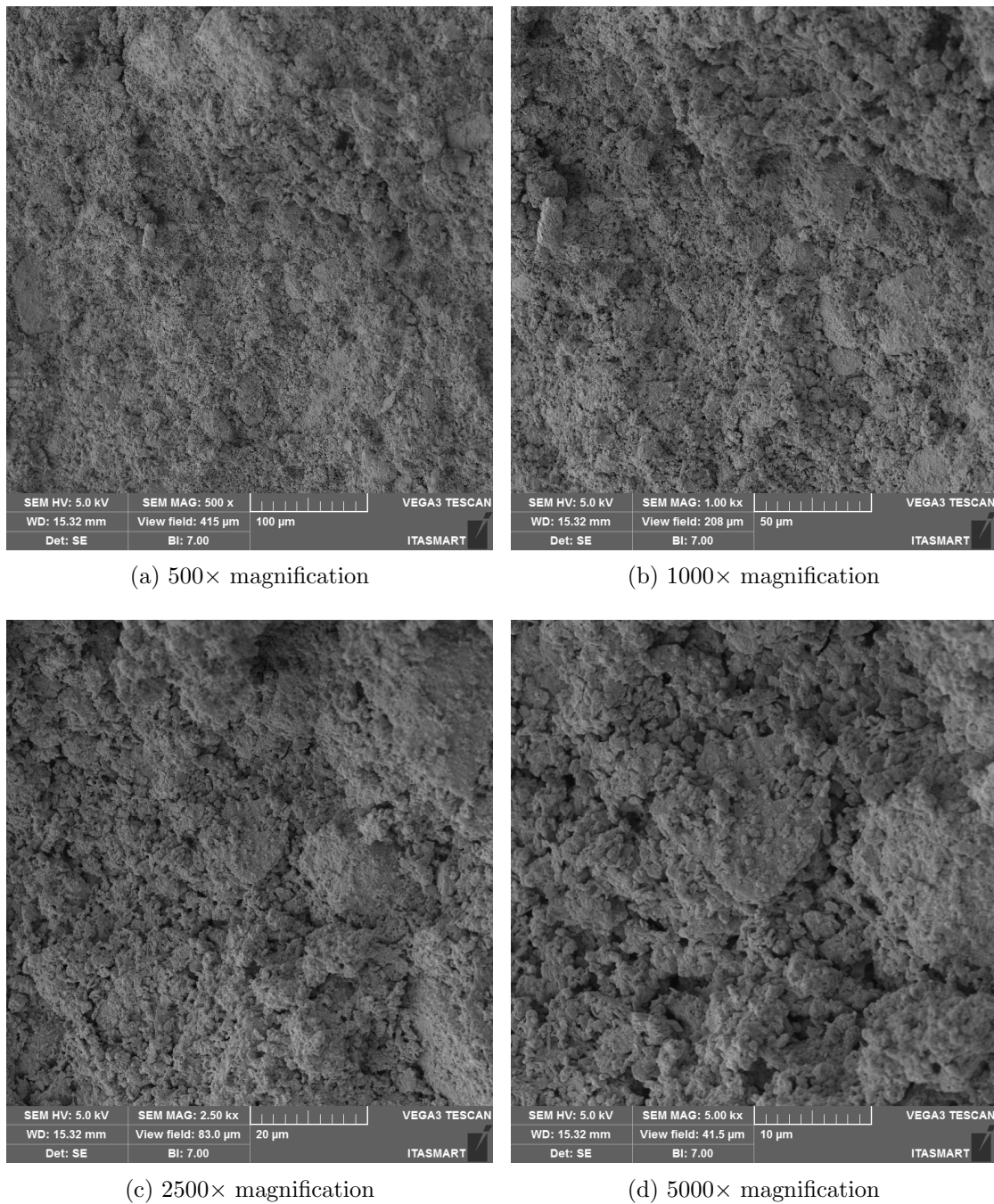


FIGURE B.1 – SEM micrographs of Spot 1, Si/Al = 0.9, cured for 3 days at 60°C.

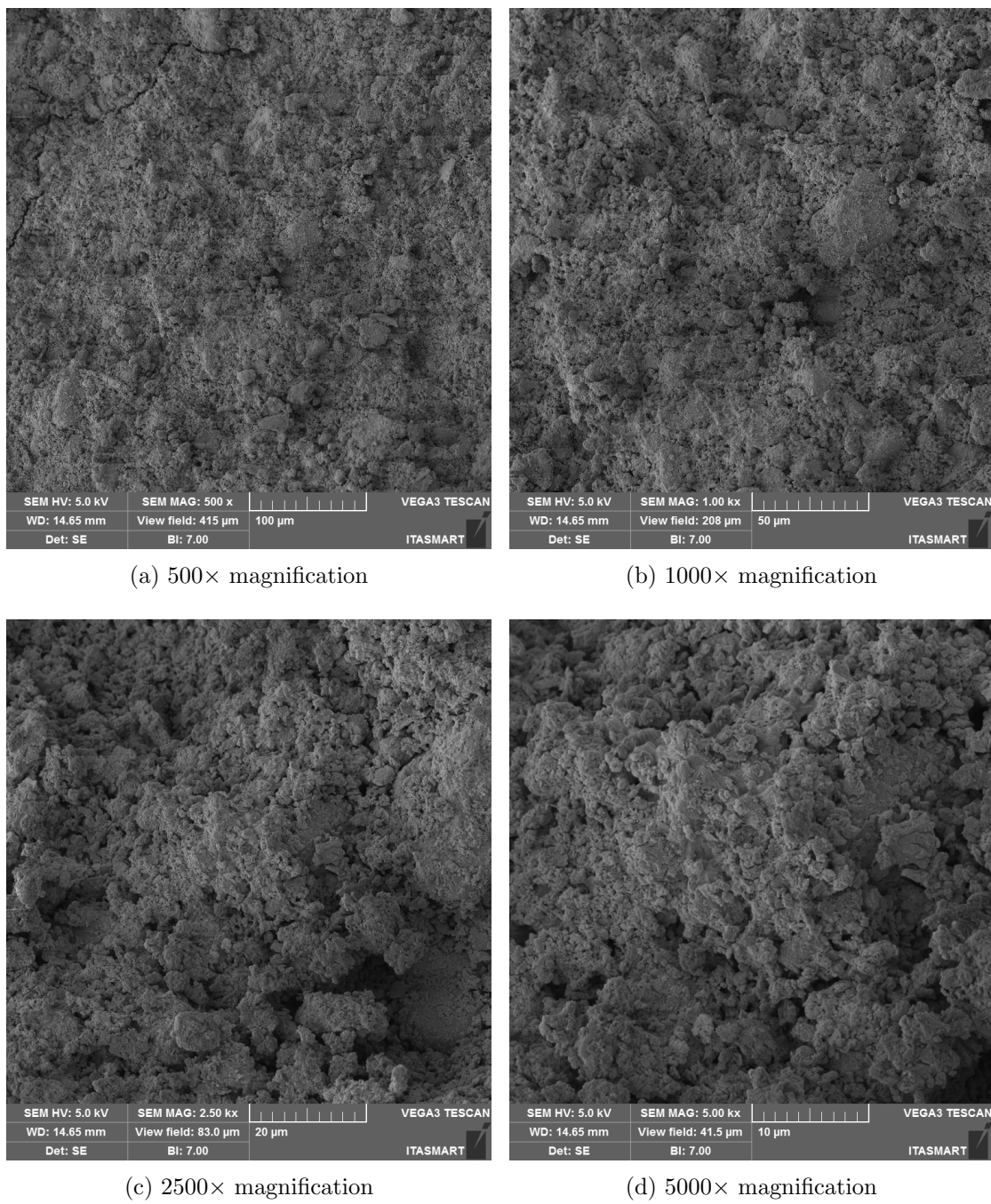


FIGURE B.2 – SEM micrographs of Spot 2, Si/Al = 0.9, cured for 3 days at 60°C.

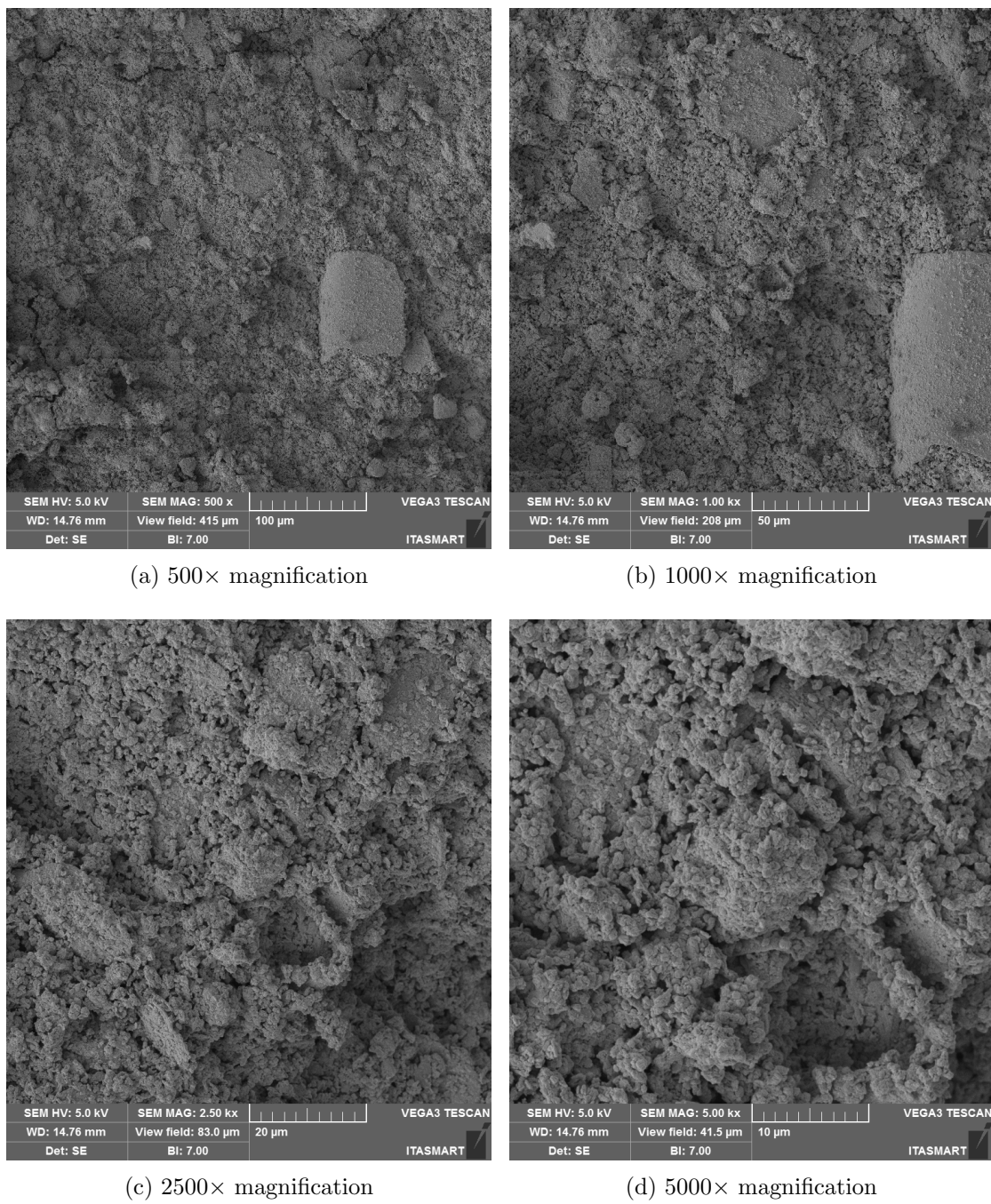


FIGURE B.3 – SEM micrographs of Spot 3, Si/Al = 0.9, cured for 3 days at 60°C.

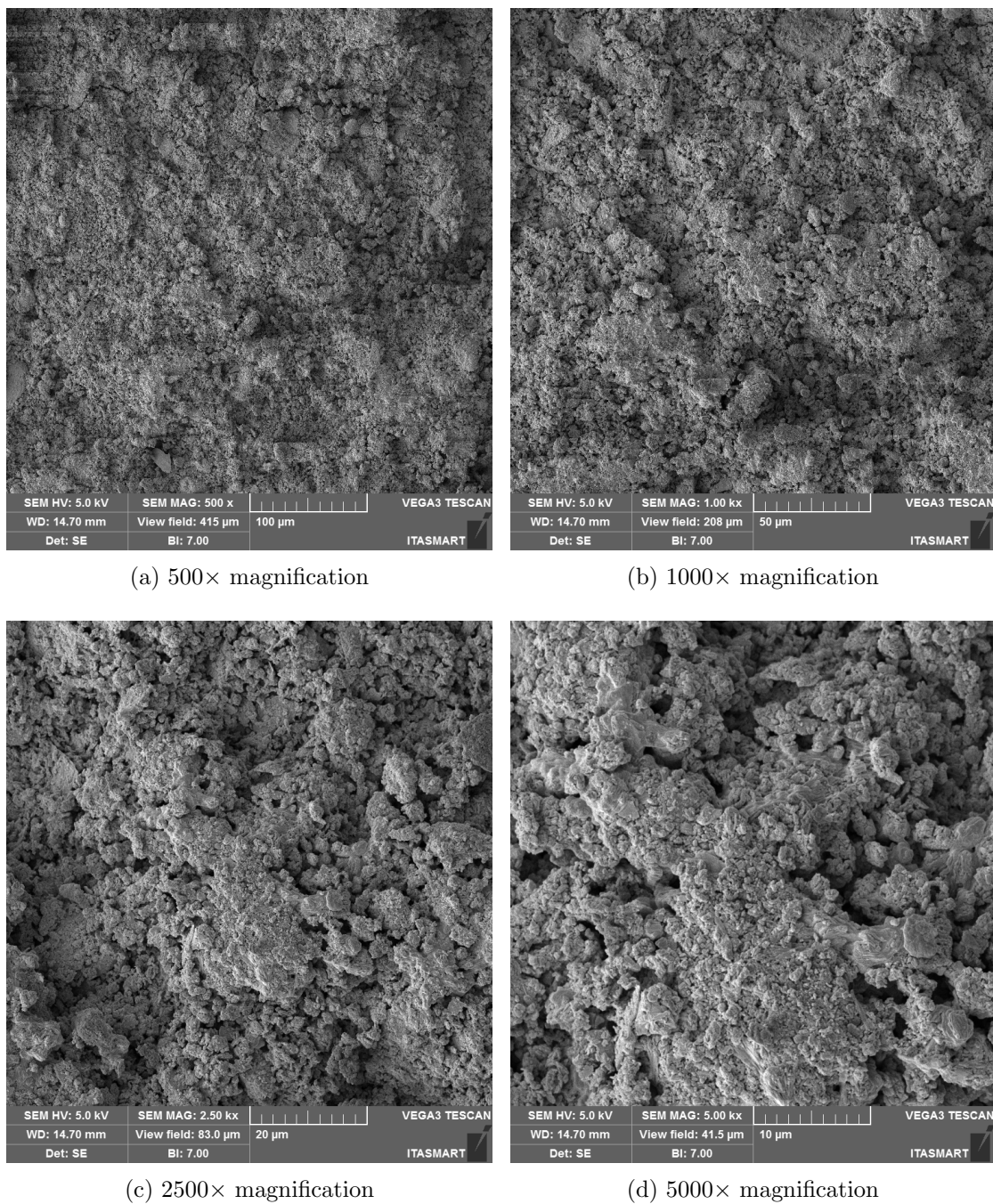


FIGURE B.4 – SEM micrographs of Spot 4, Si/Al = 0.9, cured for 3 days at 60°C.

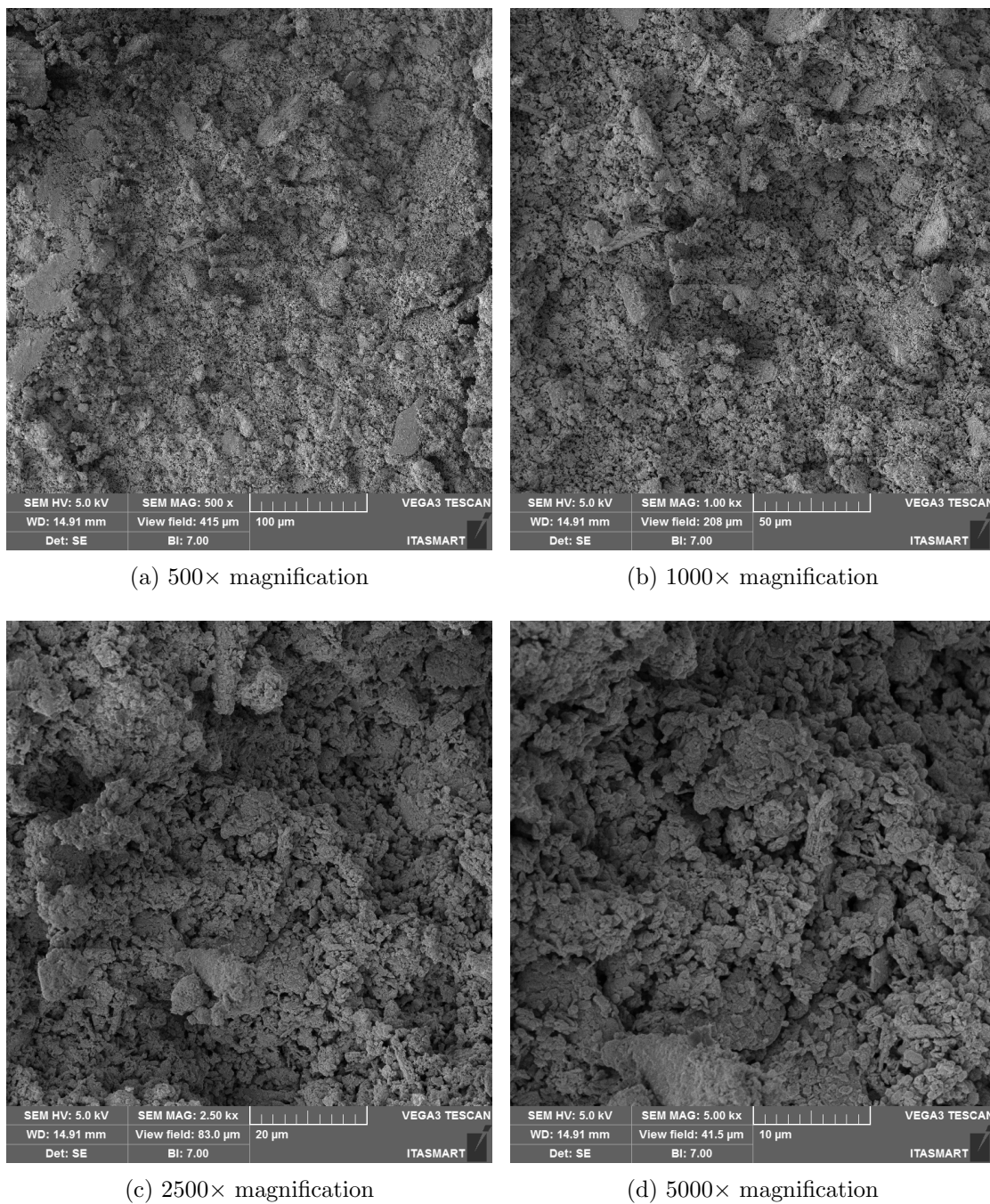


FIGURE B.5 – SEM micrographs of Spot 5, Si/Al = 0.9, cured for 3 days at 60°C.

B.2 Si/Al = 3.0

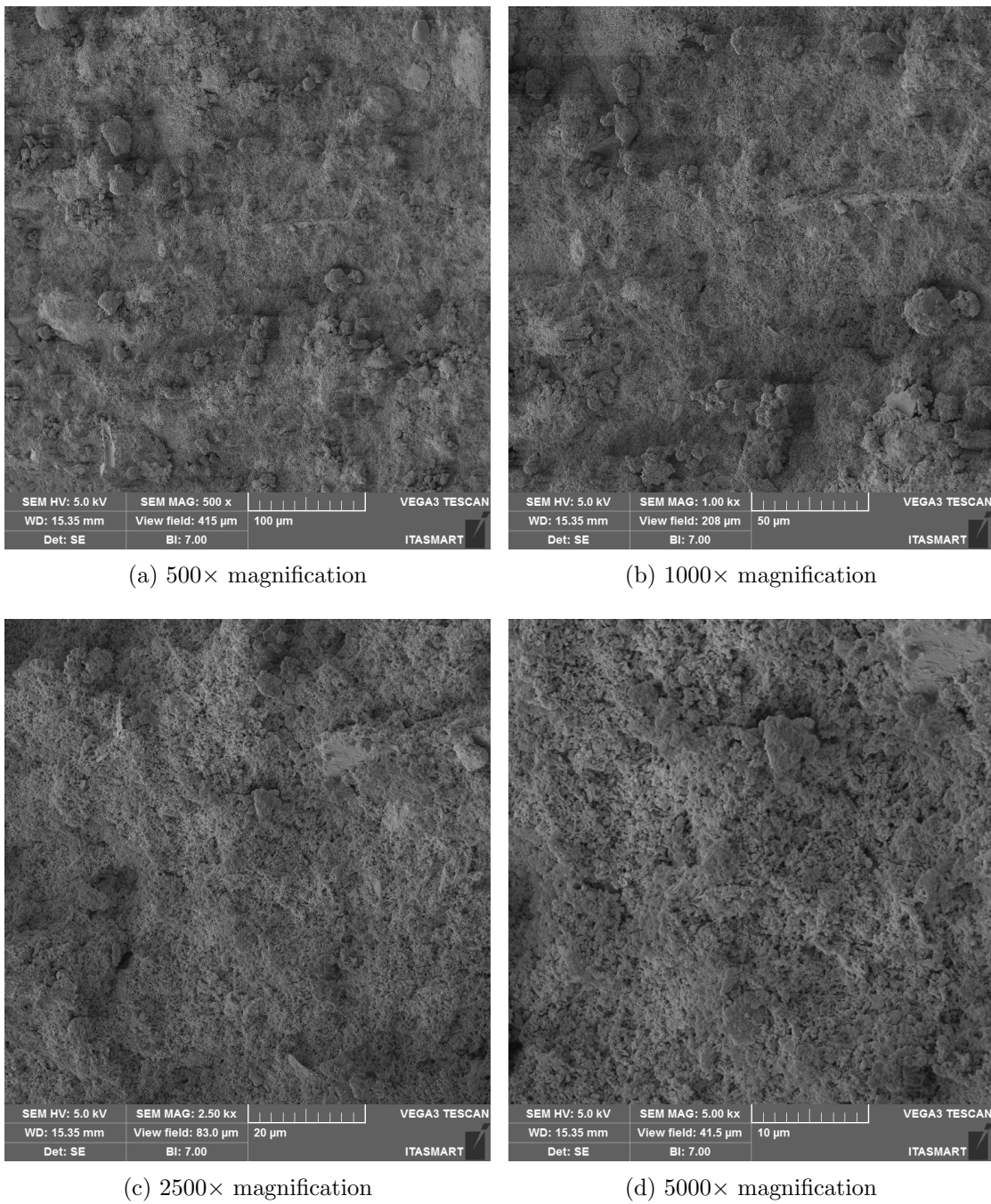


FIGURE B.6 – SEM micrographs of Spot 1, Si/Al = 3.0, cured for 3 days at 60°C.

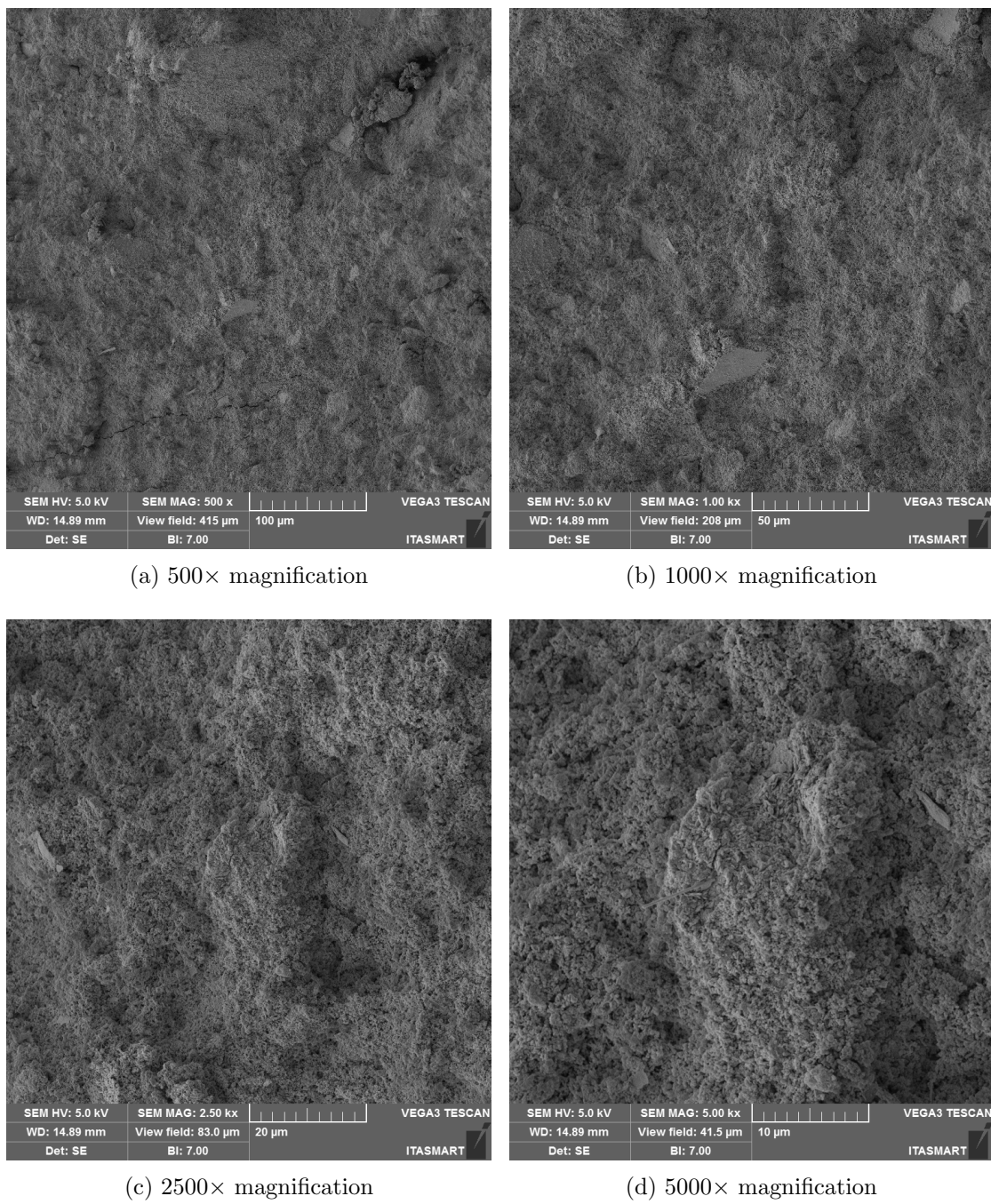


FIGURE B.7 – SEM micrographs of Spot 2, Si/Al = 3.0, cured for 3 days at 60°C.

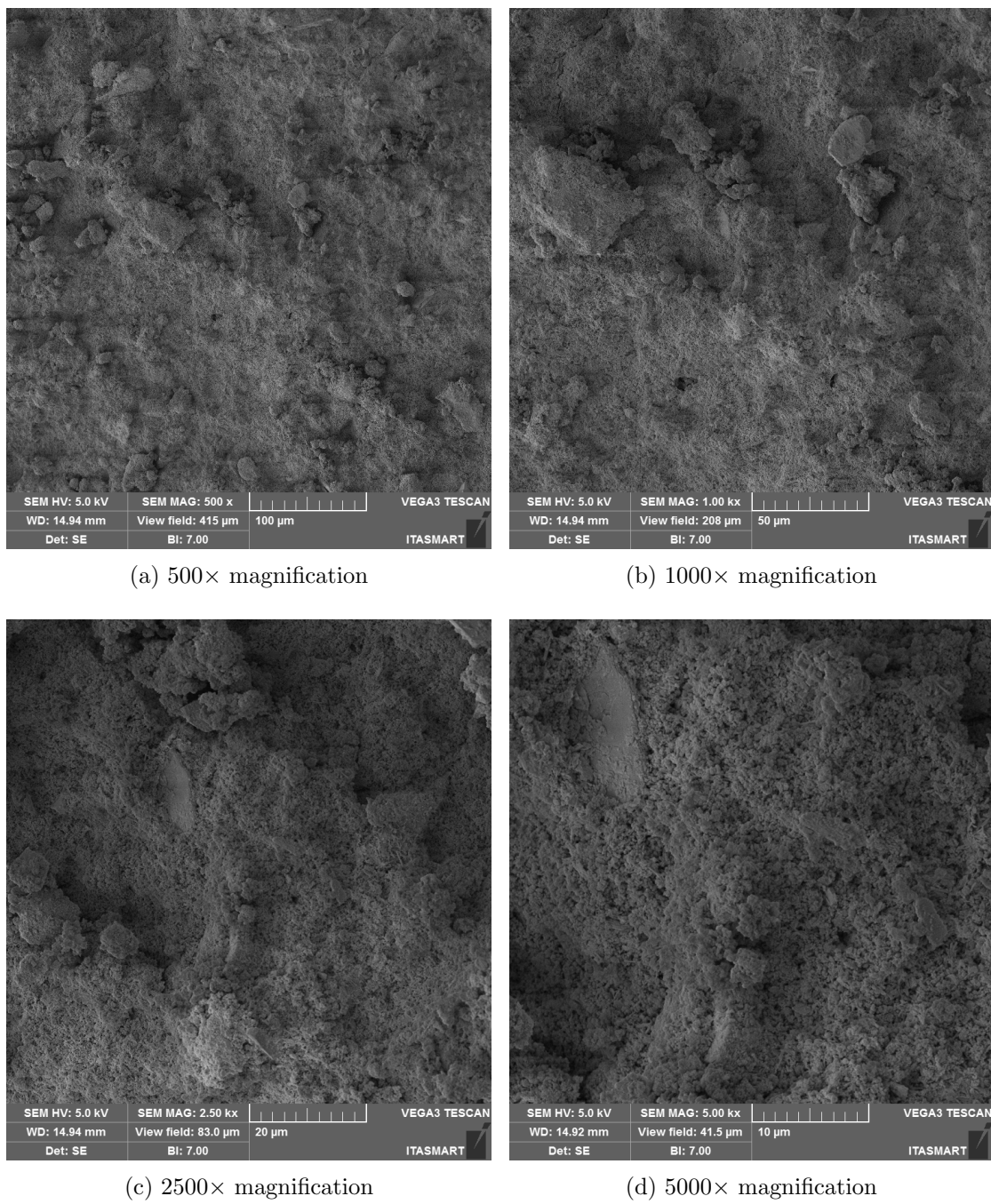


FIGURE B.8 – SEM micrographs of Spot 3, Si/Al = 3.0, cured for 3 days at 60°C.

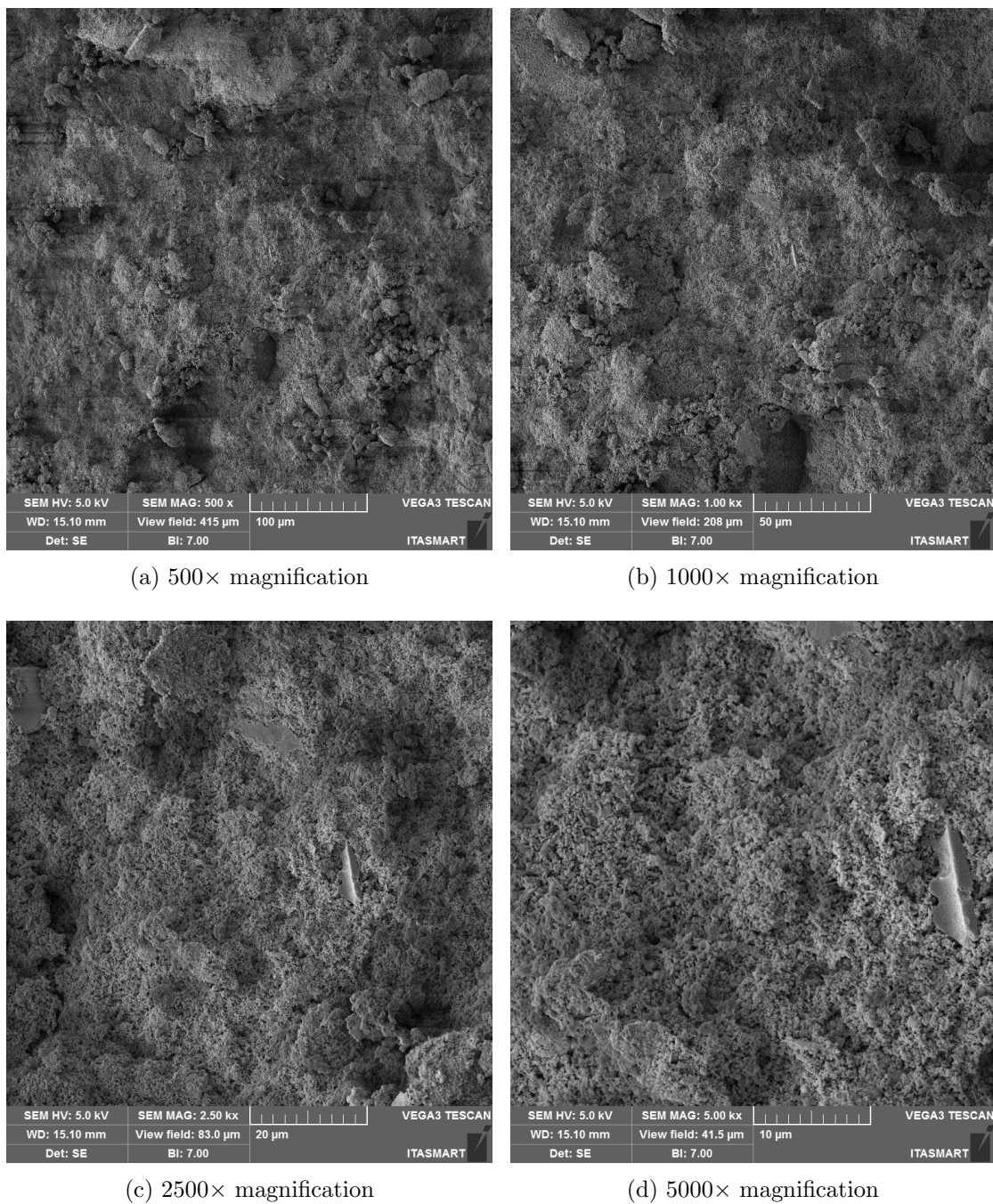


FIGURE B.9 – SEM micrographs of Spot 4, Si/Al = 3.0, cured for 3 days at 60°C.

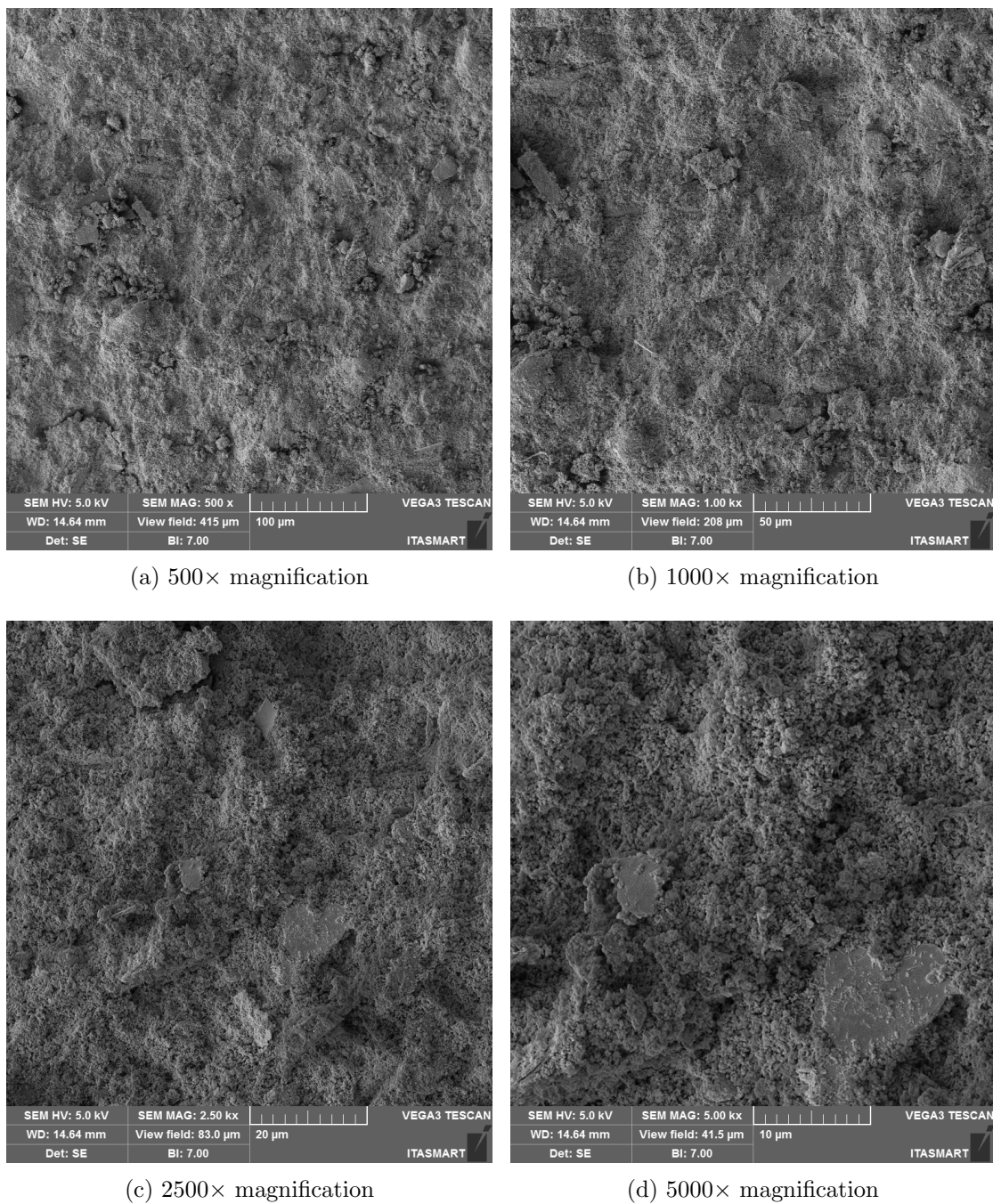


FIGURE B.10 – SEM micrographs of Spot 5, Si/Al = 3.0, cured for 3 days at 60°C.

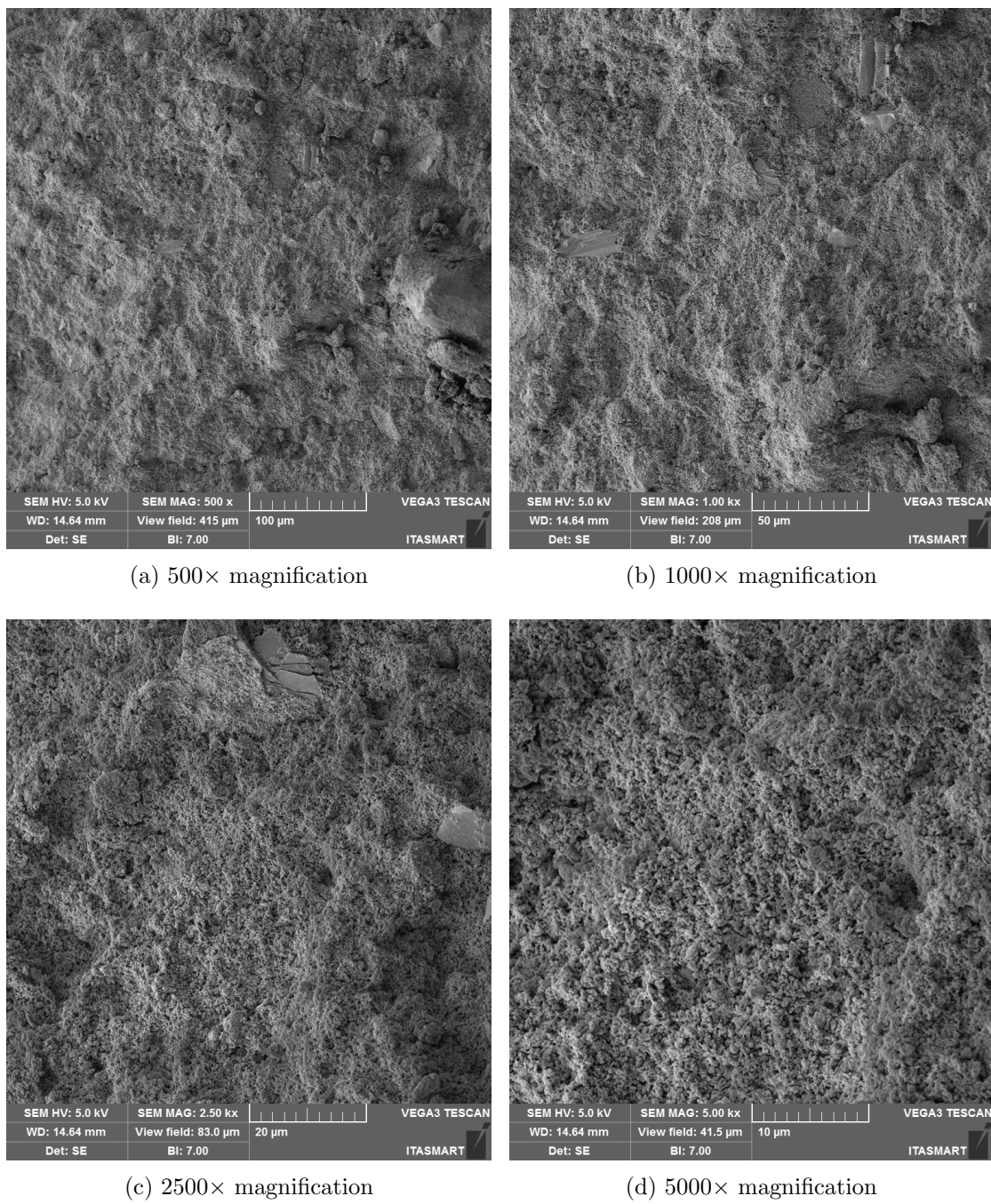


FIGURE B.11 – SEM micrographs of Spot 6, Si/Al = 3.0, cured for 3 days at 60°C.

B.3 Si/Al = 5.0

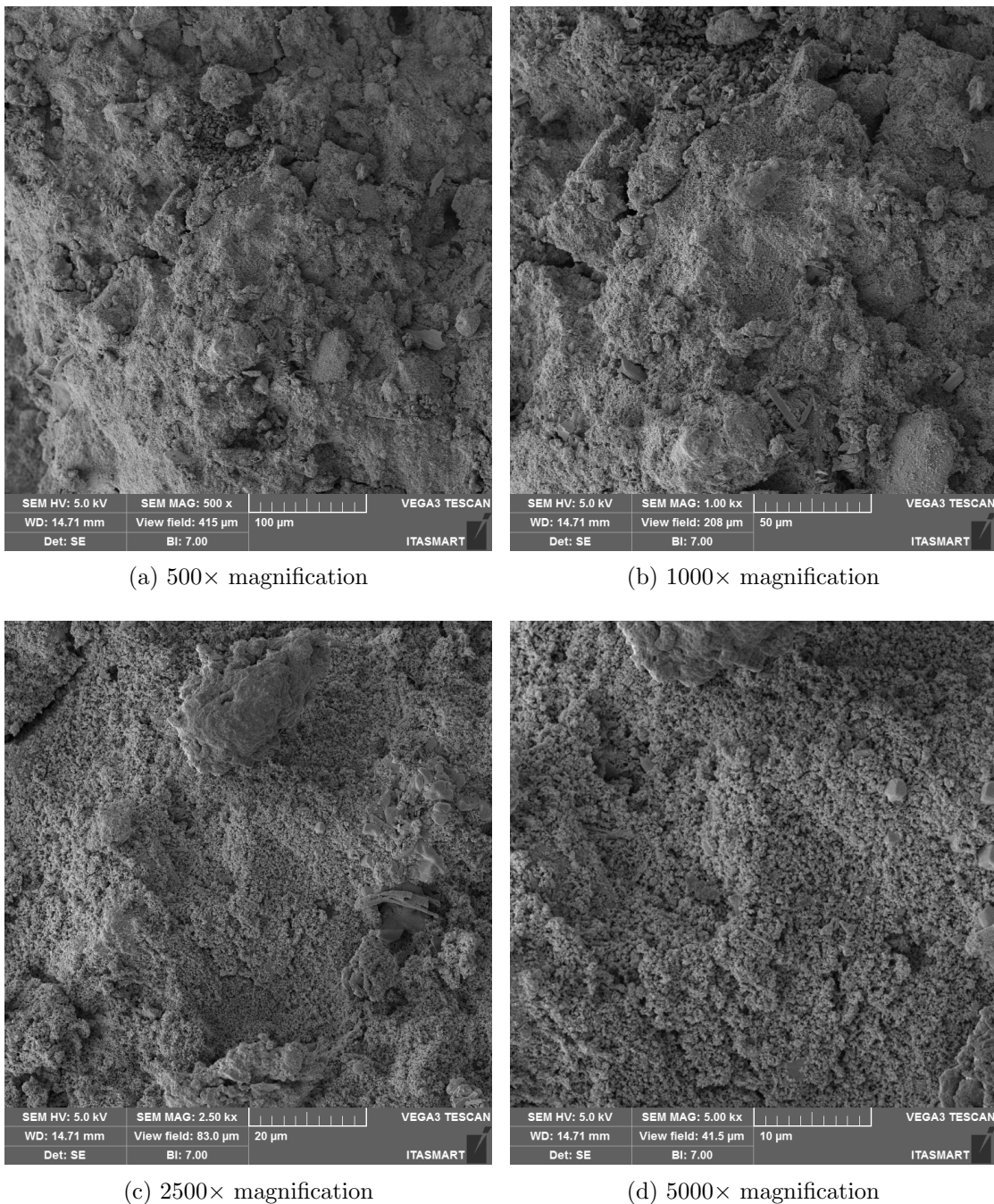


FIGURE B.12 – SEM micrographs of Spot 1, Si/Al = 5.0, cured for 3 days at 60°C.

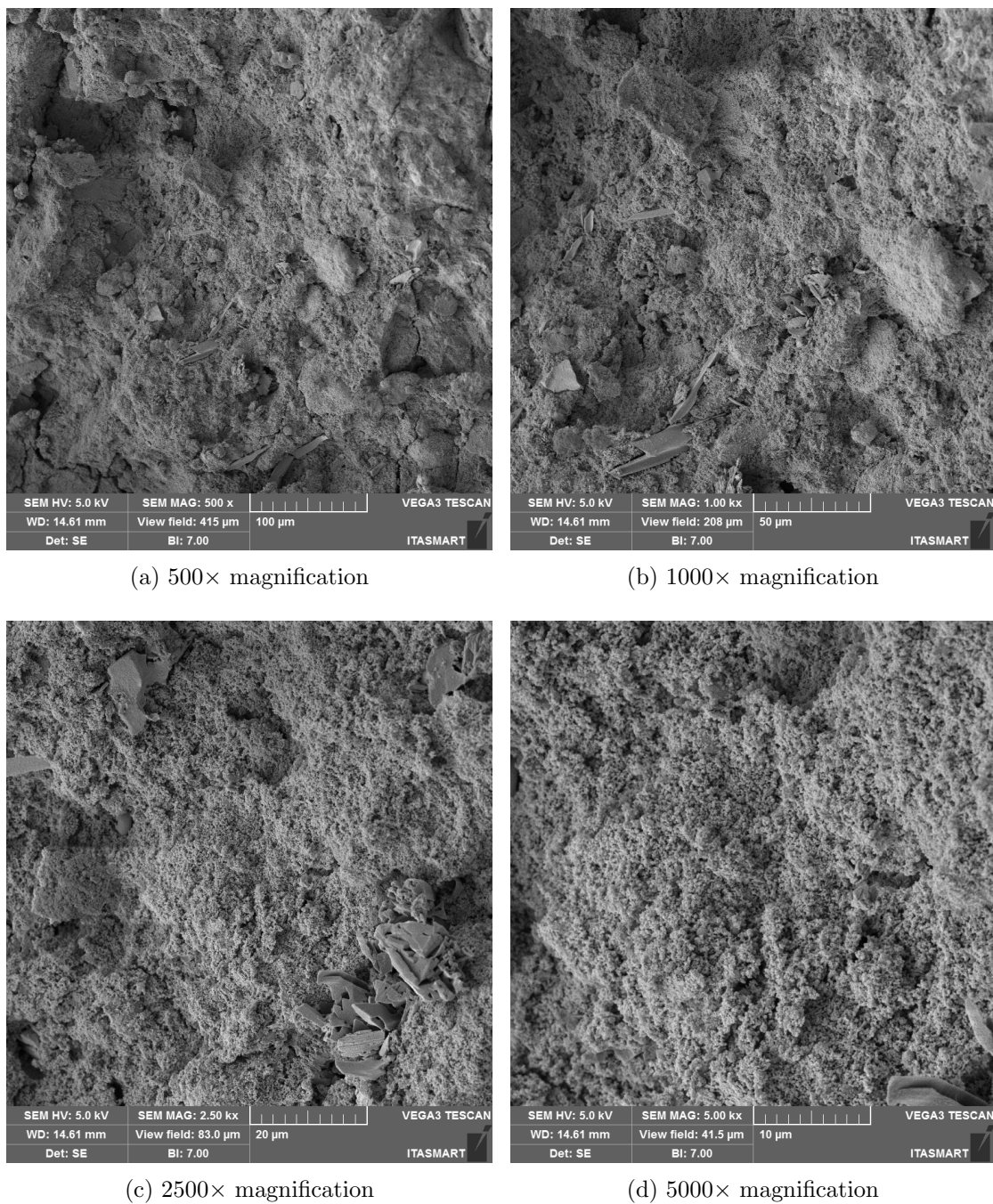


FIGURE B.13 – SEM micrographs of Spot 2, Si/Al = 5.0, cured for 3 days at 60°C.

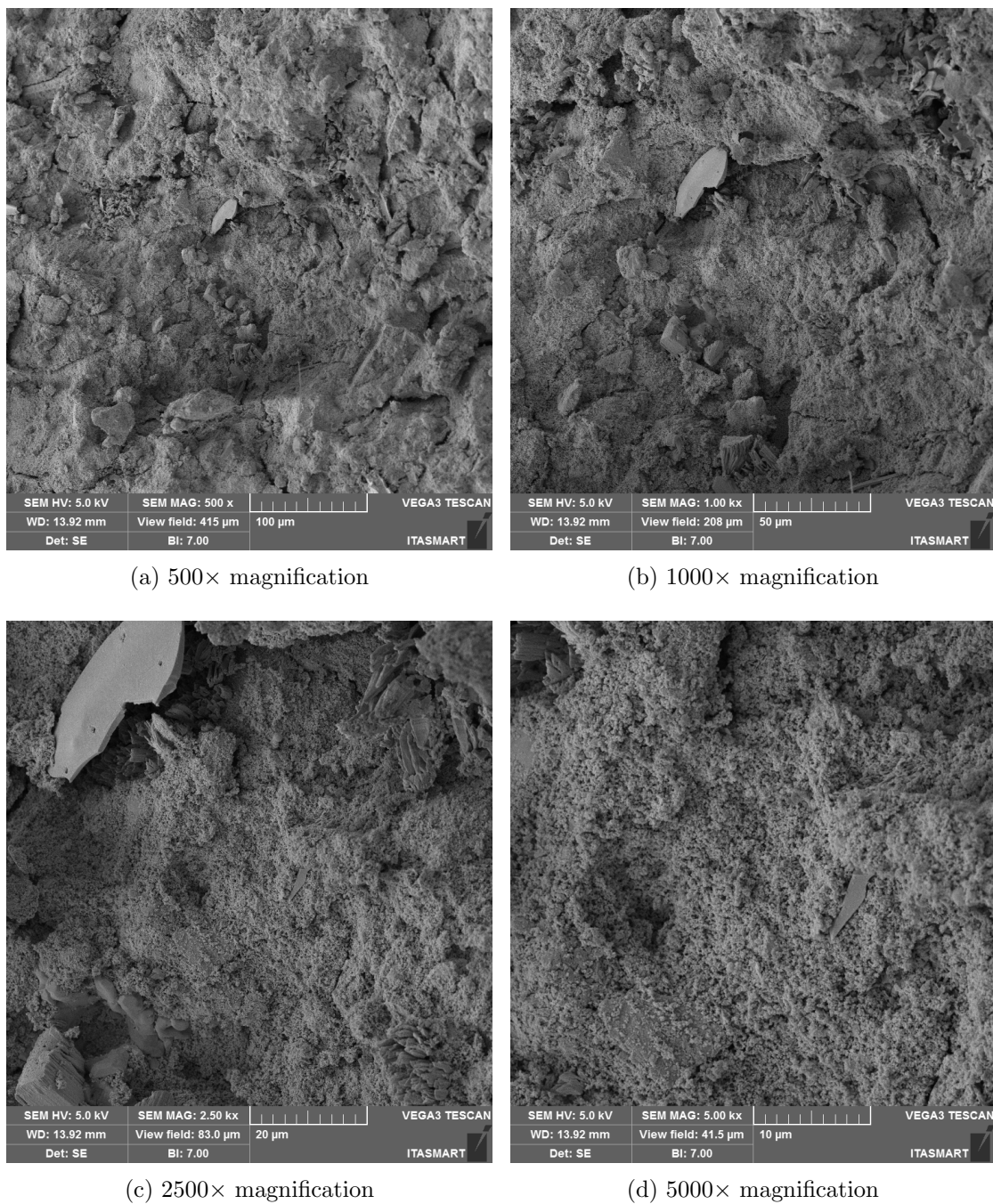


FIGURE B.14 – SEM micrographs of Spot 3, Si/Al = 5.0, cured for 3 days at 60°C.

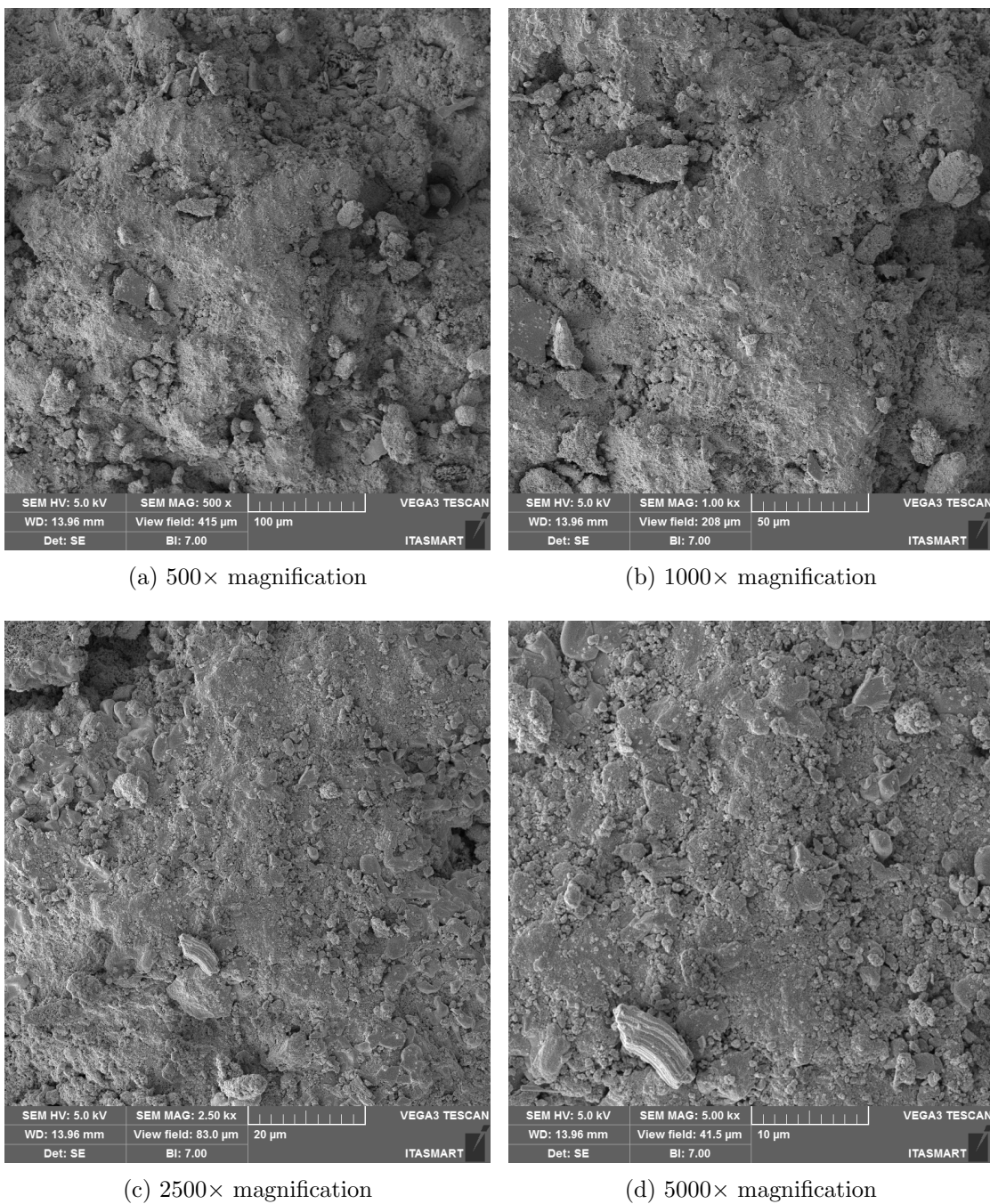


FIGURE B.15 – SEM micrographs of Spot 4, Si/Al = 5.0, cured for 3 days at 60°C.

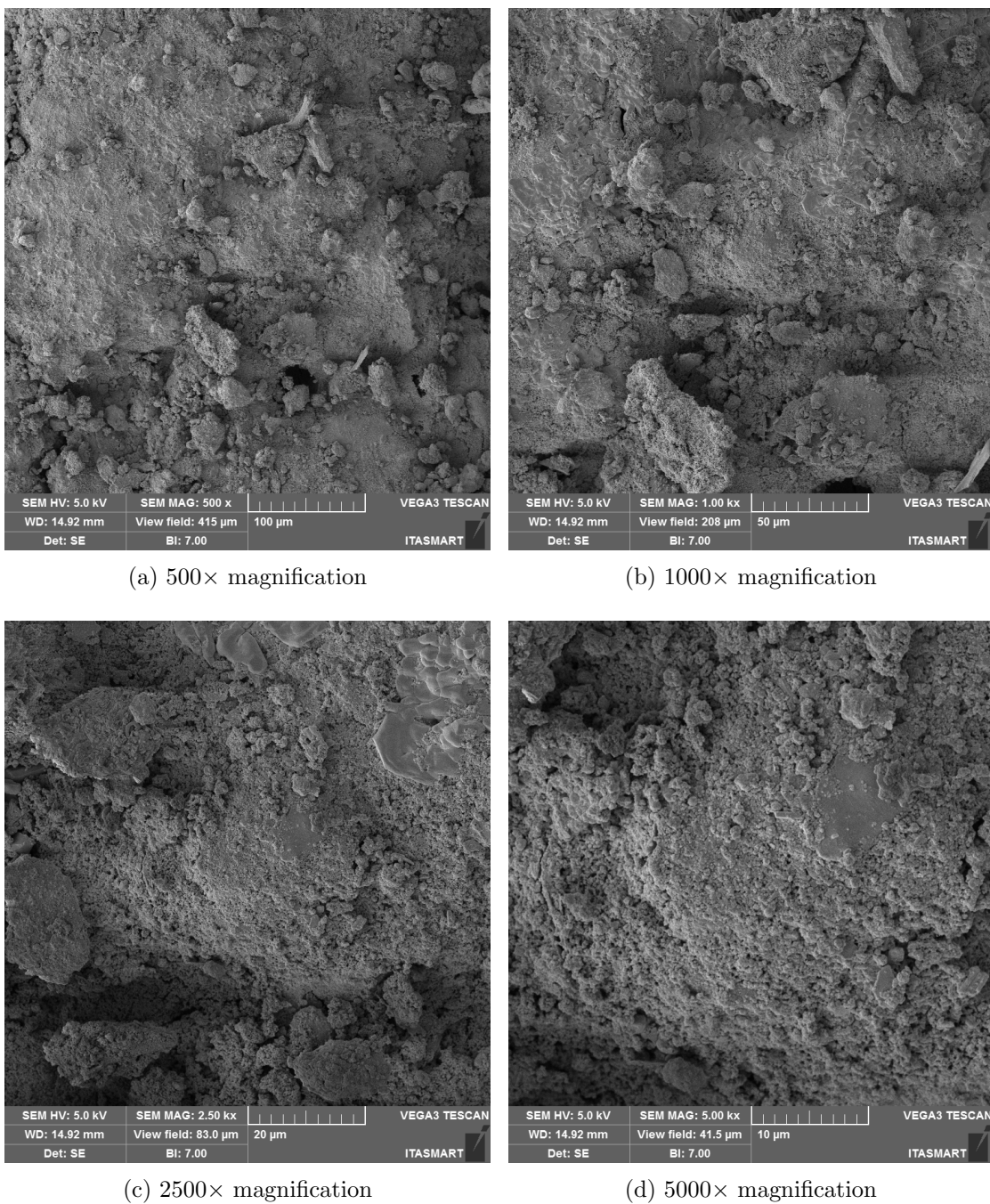


FIGURE B.16 – SEM micrographs of Spot 5, Si/Al = 5.0, cured for 3 days at 60°C.

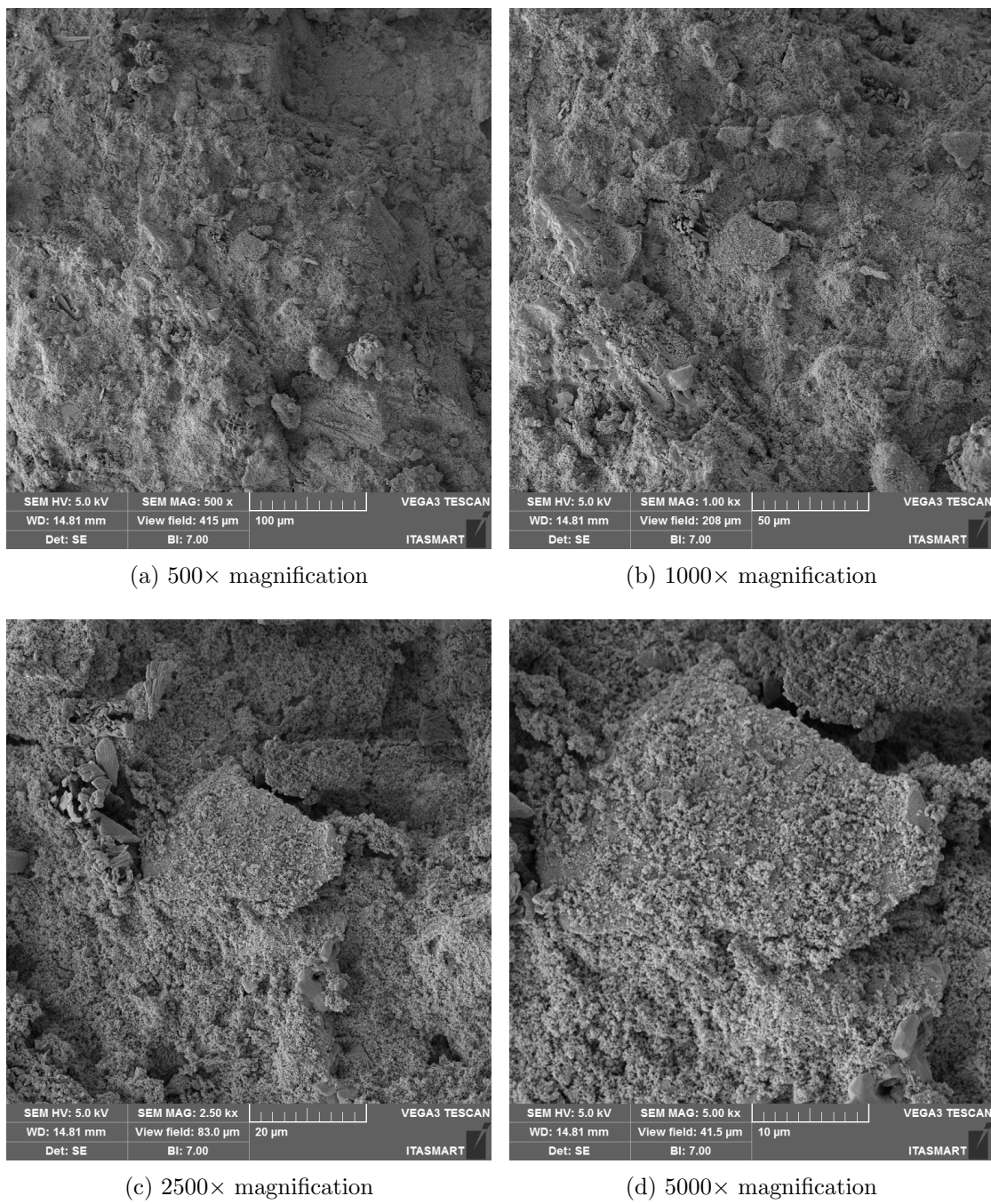


FIGURE B.17 – SEM micrographs of Spot 6, Si/Al = 5.0, cured for 3 days at 60°C.

Appendix C - EDS Spectra

This appendix presents the complete collection of EDS images for all analyzed spots across different Si/Al ratios. All specimens were cured for 3 days at 60°C and 1000× magnification. For each Si/Al ratio, atomic and weight percentages spectra are provided for each analyzed spot.

C.1 Si/Al = 0.9

TABLE C.1 – EDS spectrum of Si/Al = 0.9 pastes after 3 days of curing at 60°C.

Sample	At(%)				Wt(%)			
	Si	Al	K	Ca	Si	Al	K	Ca
0.9_60C_3d_Spot1	22.9	26.6	34.1	16.4	19.1	21.4	39.9	19.6
0.9_60C_3d_Spot2	26.5	28.9	31.1	13.7	22.7	23.7	36.9	16.7
0.9_60C_3d_Spot3	26.1	28.7	32.1	13.0	22.3	23.6	38.2	15.9
0.9_60C_3d_Spot4	24.9	28.2	32.8	14.0	21.1	23.0	38.8	17.0
0.9_60C_3d_Spot5	26.4	27.1	30.4	16.0	22.4	22.1	36.0	19.5

C.2 Si/Al = 3.0

TABLE C.2 – EDS spectrum of Si/Al = 3.0 pastes after 3 days of curing at 60°C.

Sample	At(%)				Wt(%)			
	Si	Al	K	Ca	Si	Al	K	Ca
3.0_60C_3d_Spot1	56.9	13.8	19.5	9.9	51.1	11.9	24.3	12.7
3.0_60C_3d_Spot2	59.1	13.4	18.1	9.4	53.5	11.6	22.7	12.1
3.0_60C_3d_Spot3	54.2	13.5	21.5	10.8	48.2	11.5	26.6	13.7
3.0_60C_3d_Spot4	56.3	13.6	19.8	10.3	50.4	11.7	24.7	13.2
3.0_60C_3d_Spot5	56.4	13.4	20.6	9.6	50.5	11.5	25.7	12.3
3.0_60C_3d_Spot6	56.6	12.5	20.8	10.1	50.6	10.8	25.8	12.9

C.3 Si/Al = 5.0

TABLE C.3 – EDS spectrum of Si/Al = 5.0 pastes after 3 days of curing at 60°C.

Sample	At(%)				Wt(%)			
	Si	Al	K	Ca	Si	Al	K	Ca
5.0_60C_3d_Spot1	59.5	9.2	19.6	11.6	53.0	7.9	24.2	14.9
5.0_60C_3d_Spot2	61.5	10.5	18.8	9.3	55.4	9.1	23.5	11.9
5.0_60C_3d_Spot3	58.3	8.9	20.8	12.0	51.7	7.6	25.7	15.0
5.0_60C_3d_Spot4	48.5	7.7	33.3	10.4	41.4	6.4	39.5	12.7
5.0_60C_3d_Spot5	51.1	8.3	32.8	7.8	44.9	6.8	39.5	9.7
5.0_60C_3d_Spot6	58.6	9.5	21.5	10.4	52.1	8.1	26.6	13.2

Appendix D - FTIR Spectra

This appendix presents the complete collection of FTIR spectra for solid precursors.

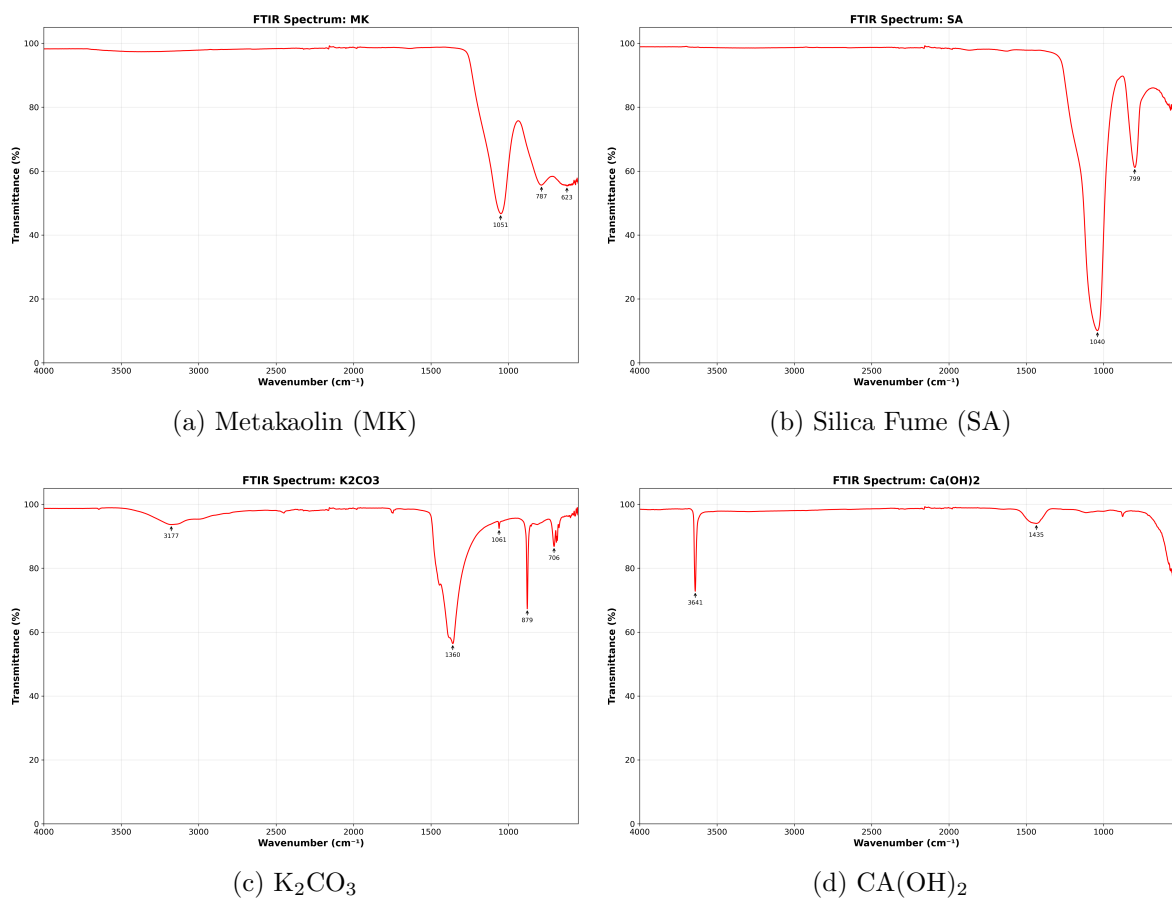


FIGURE D.1 – FTIR spectra of solid precursors.

FOLHA DE REGISTRO DO DOCUMENTO

1. CLASSIFICAÇÃO/TIPO TC	2. DATA 26 de maio de 2025	3. DOCUMENTO Nº DCTA/ITA/DM-018/2025	4. Nº DE PÁGINAS 64
5. TÍTULO E SUBTÍTULO: Development of one-part alkali-activated cement with low-calcium solid precursors and alternative alkaline sources.			
6. AUTOR(ES): Felipe Mello dos Reis			
7. INSTITUIÇÃO(ÓES)/ÓRGÃO(S) INTERNO(S)/DIVISÃO(ÓES): Aeronautics Institute of Technology – ITA			
8. PALAVRAS-CHAVE SUGERIDAS PELO AUTOR: AAM; Geopolymer; One-part			
9. PALAVRAS-CHAVE RESULTANTES DE INDEXAÇÃO: AAM; Geopolymer; One-part			
10. APRESENTAÇÃO: <input checked="" type="checkbox"/> Nacional <input type="checkbox"/> Internacional ITA, São José dos Campos. Undergraduate Course. Undergraduate Program in Civil-Aeronautical Engineering. Department of Structures and Buildings. Advisor: Prof. Dr. João Cláudio Bassan de Moraes. Co-advisor: Pamela Rodrigues Passos Severino. Defense on 05/26/2025. Published on 05/26/2025.			
11. RESUMO: Na busca por alternativas mais sustentáveis ao cimento Portland, os cimentos ativados alcalinamente têm sido amplamente estudados. Inicialmente, a maioria dos processos de mistura ocorre em duas etapas, que sacrificam a eficiência produtiva em função das melhores propriedades mecânicas. Com o objetivo aumentar a escalabilidade do processo, o desenvolvimento de sistemas monocomponentes trouxe uma tecnologia mais acessível e prática para a indústria. Ainda assim, os estudos atuais se concentram em precursores ricos em cálcio, enquanto o uso de fontes alcalinas tradicionais apresenta desafios relacionados à segurança e ao custo. Este trabalho propõe o desenvolvimento de um cimento ativado alcalinamente monocomponente utilizando precursores sólidos de baixo teor de cálcio, como sílica ativa e metacaulim, e fontes alcalinas mais seguras e acessíveis, como carbonato de potássio e hidróxido de cálcio, garantindo resistência mecânica adequada e maior viabilidade para aplicação na construção civil.			
12. GRAU DE SIGILO: <input checked="" type="checkbox"/> OSTENSIVO <input type="checkbox"/> RESERVADO <input type="checkbox"/> SECRETO			